Localisation and Transport in Driven Quantum Systems

A Thesis

submitted to the
Indian Institute of Science Education and Research Pune
in partial fulfillment of the requirements for the
BS-MS Dual Degree Programme

by

Vikram Ravindranath
20141055
Department of Physics
IISER, Pune

under the supervision of

M. S. Santhanam
Associate Professor
Department of Physics
IISER, Pune

Certificate

This is to certify that this dissertation entitled Localisation and Transport in Driven Quantum Systems towards the partial fulfilment of the BS-MS dual degree programme at the Indian Institute of Science Education and Research, Pune represents study/work carried out by Vikram Ravindranath at the Indian Institute of Science Education and Research under the supervision of M. S. Santhanam, Associate Professor, Department of Physics, during the academic year 2018-2019.

20/3/2019
Vikram Ravindranath
Department of Physics
IISER, Pune

20/3/2019
M. S. Santhanam
Associate Professor
Department of Physics
IISER, Pune

Declaration

I hereby declare that the matter embodied in the report entitled Localisation and Transport in Driven Quantum Systems are the results of the work carried out by me at the Department of Physics, Indian Institute of Science Education and Research, Pune, under the supervision of M. S. Santhanam and the same has not been submitted elsewhere for any other degree.

20|3|2019
Vikram Ravindranath
Department of Physics
IISER, Pune

Santhanam
20|3|2019
M. S. Santhanam
Associate Professor
Department of Physics
IISER, Pune

Acknowledgments

The mark of a good mentor is one who pushes you when you perform below your potential, but one who affords you the freedom to explore new avenues and truly learn. For this, if it is in this protégé’s place to say, I would like to thank Dr. Santhanam for 3 years of mentorship and what must feel like æons more of patience. I have learnt from him what it means to be a thorough investigator, and have benefited greatly from the plethora of discussions we have had, on diverse topics. I thank Dr. Harshini Tekur for her great forbearance in helping me execute code on systems under her custody, withstanding my caprices as she was wrapping up her PhD.

I owe gratitude to Dr. Sreejith GJ, my TAC member, for spending long, tedious hours helping me troubleshoot both analyses and code. Without the insights that he offered and his directions for new pursuits, this project would not have been nearly as complete, nor would I have learnt a great deal of what I am now grateful to know. I am indebted to Professor G. Ambika who guided me through my first steps into the fascinating world of chaos; she is in no small part responsible for my being taken with it. I am also thankful to Dr. Bhas Bapat and Dr. Sudarshan Ananth for their willingness to entertain discussions at length, and for their advise on several academic matters. It goes without saying that the academic environment at IISER granted me exposure to pursue topics at the forefront of research, augmented by some of the best teachers I have had.

On a personal note, a thesis year needs a bulwark against the myriad stresses with which it is synonymous. I am immensely grateful to have had Shraddha, with her antics, caring and wisdom, my parents, with their inexhaustible encouragement, my sister, who looks out for me unceasingly, and John, with his embodiment of reliability and creative expression. For many discussions, intellectual or otherwise, scientific or only tangential, I am thankful to fellow batchmates Aanjaneya Kumar and Ramesh Chandra.

Abstract

Noise is often seen as a source of unwanted decoherence in quantum systems, but this need always not be the case. In this thesis, numerical investigations of the dynamics of a quantum model that shows a localisation transition are carried out, and the effects of noise on the transport and localisation are studied. Sharp dynamical transitions as well as robustness to decoherence are found, along with a tunability of dynamics solely by noise, even when a translationally invariant model is considered, offering novel opportunities for Floquet engineering. Numerical estimates and hypotheses are made for the conditions that enable the observed phenomena

Contents

Abstract **i**

1 Introduction **1**

2 Background **3**
2.1 Floquet Basics . . . 3
2.2 Metal-Insulator Transitions . . . 5

3 Model and Implementation **8**
3.1 Model - Kicked Aubry-André-Harper . . . 8
3.2 Quantities of Interest . . . 10
3.2.1 Spectral Properties . . . 10
3.2.2 Dynamics . . . 11
3.3 Technical Details and Implementation . . . 12

4 Results and Discussion **13**
4.1 Level Statistics . . . 13
4.2 Dynamics . . . 16
4.2.1 AAH Model . . . 16
4.2.2 Translationally Invariant Models . . . 22
4.2.3 Fidelity . . . 29
4.2.4 Analysis . . . 32
4.2.5 Role of Noise Correlations . . . 36

5 Take-aways and Outlook **40**

Appendices **43**

A Code to Calculate Spread **43**

List of Figures

4.1 Distribution of level spacing ratio r for the kicked system 14
4.2 Statistical properties of the (noisy) evolution operator 15
4.3 Density profile and spread of the wavefunction for protocol (C) 16
4.4 σ^2 vs. t/τ at $A = 10, 100$ for uniform noise 17
4.5 σ^2 vs. t/τ for uniformly drawn kick times 18
4.6 σ^2 vs. t/τ at $\lambda = 0.5, 10$ for Poisson noise 19
4.7 σ^2 vs. t/τ for Poisson kick times 20
4.8 σ^2 vs. t/τ at $\beta = 0.5, 10$ for Normal noise 20
4.9 σ^2 vs. t/τ for Normal kick times 21
4.10 σ^2 vs. t/τ at $A = 10, 100$ for 2, 3-band models 22
4.10 σ^2 vs. t/τ at $A = 10, 100$ for a 4-band model 23
4.11 σ^2 vs. t/τ at $V = 1.5$ for a 3, 4-band model 23
4.12 σ^2 vs. t/τ for uniformly drawn kick times, 2-band 24
4.13 σ^2 vs. t/τ at $V = 1.5$ for 3, 4-band models for Poisson noise 24
4.14 σ^2 vs. t/τ at $\lambda = 0.5, 10$ for 2, 3, 4-band models with Poisson noise 25
4.15 Band structures for the 2-band model 26
4.16 Band structures for the 4-band model 27
4.17 Special case of flat bands 28
4.18 Evolution of fidelity, with uniform noise 29
4.19 Evolution of fidelity, with Poisson noise 30
4.20 γ_4 vs. t/τ for uniformly drawn kick times 32
4.21 γ_4 vs. t/τ for uniformly drawn kick times, 2-band model 33
4.22 γ_4 vs. t/τ for Poisson kick times, 2-band 34
4.23 Fits σ^2 vs. t/τ at $A = 10, 50, 100$ for the AAH model, with uniform noise 35
4.24 Intermediate regimes for the AAH Model 36
4.25 σ^2 vs. t/τ at $V = 1.57$ with a coin-toss 37
4.26 Exact results for the coin toss model 39

List of Tables

3.1 Descriptions of various schemes 12

Chapter 1

Introduction

With the use of ultracold atoms in experimental set-ups, the idea of a quantum simulator has been realised extensively over the past two decades or so, enabling the exploration of a diverse range of phenomena, from quantum chaos [1] to several in many-body physics [2], such as the BCS-BEC or the superfluid-Mott insulator transition. These have allowed the engineering of optical lattices with a high degree of tunability [3], offering a novel way to realise dynamics in condensed matter. More recently, the ability to manipulate many-body systems by periodic driving them has caught a great deal of attention [4]. Particularly in tight-binding systems (which are realised in the aforementioned optical lattices), this is due to the variety of properties that can be manipulated, from band topology [5] to transport and localisation [6–8].

Key to the implementation of these quantum simulators has been the degree of isolation and coherence that has been achieved with them. However, perfect isolation is practically impossible, and a coupling to an environment leads to an inevitable loss of coherence, which is often referred to as the cause for the emergence of a "classical" world from the quantum [9]. In addition to the fact that noise realises the effects of a dissipation-free coupling to the environment [10–12], it was widely thought that any minimal noise introduced into the system was likely to cause decoherence and thus, wash out the coherence that is so responsible for the quanutm phenomena that one sees. The problem is exacerbated double-fold when one considers the paradigm of manipulation of driving, wherein noise could enter either in the driving (period/amplitude) or by imperfect isolation, presenting a pressing issue in the field of Floquet engineering.[1]

Recent investigations in the quantum chaotic kicked rotor, both theoretical [13] and experimental [14], however, have shown that the status quo need not hold. It has been found that for a crucial family of stochastic influences (namely, Lévy noise, the tail of whose distribution $P(t) \sim t^{-(\beta+1)}$ at large t leads to diverging means for $\beta < 1$) that decoherence is *non-exponential*, and the accompanying transport in momentum space (energy absorption) is *subdiffusive*, in contrast to the results of [12]. It is in the light of this that this thesis has been undertaken - studying the dynamical properties of kicked tight-binding chains when the driving is aperiodic.

---

[1] It is interesting to note that Gaston Floquet was a 19th Century mathematician whose name, owing to his work on time-periodic differential equations, has become synonymous with a world of quantum phenomena, despite his passing even before the advent of the Schrödinger Equation

While often it suffices to calculate various information theoretic measures – such as *fidelity* or *purity* [15] – to observe the loss of coherence, it is more instructive to evauluate the effects of coherence loss. An appropriate candidate is that of Anderson Localisation [16], a phase coherent effect where wavepackets on a disordered lattice become exponentially localised and the diffusion is suppressed beyond the localisation length. Upon the introduction of noise into the system, should it decohere, then localisation is extenuated. The exact mechanism [17], albeit in momentum space, is responsible for the quantum localisation that is observed in the kicked rotor, which absorbs energy only for a small finite time – as opposed to the classical case, which absorbs energy indefinitely and diffusively, when the parameters of the system are such that the system is chaotic. In the rotor, this is termed dynamical localisation, which is not to be confused with dynamic localisation in [6], wherein the absence of transport is solely due to a tuning of the external driving, and not the intrinsic dynamics of the system.[2] The results of [13, 14] show that a nonexponential decoherence is innately linked to subdiffusion which is markedly different from classical behaviour.

The objective of this thesis is, then, to study the dynamics of a tight-binding chain, both with and without on-site potential (the former being the Aubry-André-Harper (AAH) Model) that give rise to a metal-insulator transition [7, 18]. Following this, Chapter 2 is a short introduction to the basics of periodically driven systems and of metal-insulator transitions in 1-D, pertinent to the topics explored in the thesis. In Chapter 3, the model is defined in some detail, along with a description of the quantities of interest and a note on the technicalities of the numerical implementation. Chapter 4 houses the results and their accompanying discussions, and Chapter 5 summarises the takeaways from this work and outlines possible future directions of exploration.

---

[2] This distinction, of course, borders on the pedantic

Chapter 2

Background

2.1 Floquet Basics

Consider a periodic, time-dependent Hamiltonian $H(t)$ such that $H(t+\tau) = H(t)$, where τ is the period of the driving. The Schrödinger Equation, evaluated for the unitary time-evolution operator U

$$\begin{aligned} &|\psi(t)\rangle = \hat{U}(t)\,|\psi(0)\rangle \\ \Longrightarrow\ &\imath\hbar\frac{\partial\,|\psi(t)\rangle}{\partial t} = \hat{H}(t)\,|\psi(t)\rangle \\ \Longrightarrow\ &\imath\hbar\frac{\partial\hat{U}(t)}{\partial t} = \hat{H}(t)\hat{U}(t), \end{aligned} \tag{2.1}$$

then, is of the *Floquet* form [19], where[1]

$$\begin{aligned} &\hat{U}(t) \equiv \hat{P}(t)e^{-\imath t\hat{R}} \\ &\hat{P}(t+\tau) = \hat{P}(t);\ \hat{P}(0) \equiv \mathbf{1} \\ &\hat{R}^{\dagger} = \hat{R} \neq \hat{R}(t). \end{aligned} \tag{2.2}$$

The eigenstates of the operator $\hat{U}(t)$ are of the form

$$|\psi(t)\rangle = e^{-\imath\varepsilon_a t}\,|u_a(t)\rangle\,;\ |u_a(t+\tau)\rangle = |u_a(t)\rangle\,, \tag{2.3}$$

$$\hat{H_F}\,|u_a(t)\rangle \equiv \left(\hat{H}(t) - \imath\frac{\partial}{\partial t}\right)|u_a(t)\rangle = \varepsilon_a\,|u_a(t)\rangle\,. \tag{2.4}$$

---

[1] $\hbar = 1$ in subsequent discussions

The veracity of these equations can be seen with the following identifications:

$$\begin{aligned}
\hat{R}\,|u_a(0)\rangle &= \varepsilon_a\,|u_a(0)\rangle \\
|u_a(t)\rangle &= \hat{P}(t)\,|u_a(0)\rangle \\
\hat{R} &= \frac{1}{\tau}\int_0^\tau \mathrm{d}t\,\hat{H}(t) \\
\hat{P}(t) &= \mathscr{T}\left\{\exp\left(-\imath\int_0^t \mathrm{d}t'\,\hat{H}(t')\right)\right\}\exp\left(\imath t\hat{R}\right)
\end{aligned} \tag{2.5}$$

The so-called *Floquet Hamiltonian* defined in Eq. (2.4) lends itself particularly well to diagonalisation via a Fourier transform, especially if $\hat{H}$ can be decomposed into an integrable $\hat{H}_0 + g(t)\hat{V}$ where $g(t+\tau) = g(t)$, and the resulting operator can be expanded in the basis of H_0. Time dependent systems are referred to as 1.5 degrees of freedom systems, because the Hamiltonian formalism for time-independent systems can be extended as follows:

$$\begin{aligned}
H &= H(p,q,t) \\
q_0 &:= t;\ p_0 := -H \\
\mathscr{H} &:= H + p_0 \\
\dot{q_0} &= \frac{\partial\mathscr{H}}{\partial p_0} = 1 \\
\dot{p_0} &= -\frac{\partial\mathscr{H}}{\partial q_0} = -\frac{\partial H}{\partial t}
\end{aligned} \tag{2.6}$$

Since the condition $p_0 = -H$ does not offer any information about the dynamics of the system, this system has 1.5 degrees of freedom. Floquet systems provide some of the simplest examples of chaos in 1-D systems, because in most 1-D systems, where energy is the only conserved quantity, the kicking eliminates its conservation. One such example is the kicked rotor [20], whose Hamiltonian is given by

$$H = \frac{p^2}{2} + K\sum_n \delta(t-n)\cos(\theta),$$

where K is the kicking strength, and the period has been set to 1. From this, the standard map

$$\begin{aligned}
p_{n+1} &= p_n + K\sin(x_n) \\
x_{n+1} &= x_n + p_{n+1}
\end{aligned} \tag{2.7}$$

is induced. For a value of $K \gtrsim 0.98$ the classical map is completely chaotic, and the momentum grows diffusively [20]. One might question the abundance of a large class of time-periodic systems – the δ-kicked systems – in literature, when such systems from the very outset seem experimental unrealisable. The reasons behind this are two-fold – one, the Floquet operator over a single period of evolution easily decomposes, allowing for analytical tractability (as will be shown in Eq. (3.2)) and two, many crucial factors of the more realistic rectangular waves or periodic driving can be captured by this idealised limit of the kicking (down to a rescaling of variables) [14, 20].

This Hamiltonian can be straightforwardly quantised. However, its phenomenology drastically changes in the quantum setting, most visibly in the growth of $\langle p^2 \rangle$, which grows as t until a time $t* > t_{\text{Ehrenfest}}$, after which it ceases to grow, instead oscillating about a mean value. This was shown to be due an Anderson localisation in momentum space [17]. As this is a phase coherent phenomenon, the persistence of this localisation under noise is of great interest.

2.2 Metal-Insulator Transitions

Band theory predictions of metallicity rely on the notion of band-filling and band-gaps [21]. Thus, whether a 1-D system, in this non-interacting framework, is a metal or an insulator depends on the system as a whole (i.e. unit cell occupation) and not much heed is paid to the Wannier states that compose the lattice[2]. Thus, in a tight-binding model without an on-site interaction term, eigenstates are all Bloch waves, delocalised over the entire lattice. When one considers the generation of Peierls defects, where atoms in an initially equally spaced 1-D lattice (of size L) are shifted (to first order) by a small amount $\pm\delta$, this can instead be considered a 1-D lattice with a basis, leading to the opening of band-gaps at $ka = \pm\frac{\pi}{2}$. Via an elegant transfer matrix mechanism, it can be shown [22] that states with energies in the band-gap decay exponentially. An introduction of an impurity in the system can facilitate such a bound state as an eigenstate of the system.

Taking this idea further, one notices an intuitive reason for Anderson localisation, namely that the introduction of more and more impurities leads to the presence of more states in the gap – essentially a breaking up of the energy levels from bands into a discrete spectrum [22]. Anderson localisation in 1-D however, is manifest for arbitrarily small disorder in less than 3 dimensions. The caveat in the previous explanation lies in the fact that the strength of disorder is independent of the number of disorder events in the lattice. When it so happens, that even within the tight-binding approximation, that all the states are exponentially localised, the conduction of such systems drops, effectively rendering them insulators, but unlike band-insulators of the preceeding paragraph, the insulation arises not from macroscopic consideration of band filling, but the localisation of each of the emergent eigenstates.

---

[2] Or the *AO*s in LCAO

In truth, such a qualitative explanation, in terms of a decimation of the bands, works far better for the case of the Aubry-André-Harper (AAH) model, which, unlike the Anderson model, shows a Metal-Insulator transition. Its Hamiltonian is given by

$$\begin{aligned} H &= -J\sum_{i=1}^{L}\left(c_i^\dagger c_{i+1} + c_{i+1}^\dagger c_i\right) + \sum_{i=1}^{L} V_i c_i^\dagger c_i, \\ V_j &= V\cos(2\pi\alpha j + \phi), \end{aligned} \tag{2.8}$$

where α is a modulation parameter which decides how the potential aligns with the underlying lattice, V is the strength of the potential and J is the hopping amplitude between nearest neighbours.

When $\alpha = \frac{\sqrt{5}-1}{2}$, the model is completely quasiperiodic and is paradigmatic of correlated disorder. The critical point $V/J = 2$ shows multifractality in the eigenstates, diffusive dynamics and a fractal spectrum, above which the eigenstates are localised and below which, they are extended. The evolution of the spectrum as one increased V follows the qualitative picture delineated above [23] – for small V, the spectrum is still composed of bands, with greater and greater decimation as V increases, until, at the critical point, there is an uncountable set of breaks inserted into the spectrum, quite like a Cantor set. Above criticality, the eigenvalues become discrete and hence, their states localised. It is often quoted that the critical point can be obtained by means of a Fourier transform which establishes a momentum space-position space duality; however, there is nothing special to this sort of duality since all tight-binding models with a cosine potential are manifestly self-dual [18].

While the model is often referred to in literature largely by the names of Serge Aubry and Gilles André, who proposed it as a model of an Anderson localisation transition in 1-D [18], it was originally PG Harper [24, 25] who found that it emerged as a model to study the spectral properties of electrons in lattices under the influence of a uniform magnetic field. In this case, $\alpha = \frac{ea^2H}{\hbar c}$, where a is the lattice spacing and H the applied magnetic field. This model achieved its heights of fame with the publishing of Hofstadter's 1976 paper [26], who studied the electronic motion in a 2-D lattice under a uniform, perpendicular, magnetic field, from which arose the Aubry-André-Harper model[3] at $V = 2$. He found that for irrational α, the spectrum was a fractal[4], a statement that today has firm mathematical standing [28], and stronger conditions of α – namely, that it be *Diophantine*, which is to say that rational approximates to this number must converge extremely slowly. The butterfly itself has been realised experimentally, in a set-up of scatterers [29] in which the transmission of microwaves follows the same transfer matrix as induced from the Harper Model, and more recently, in graphene superlattices and heterostructures [30–32]. Moving away from spectral properties, the localisation-delocalisation transition itself has been observed in a photonic lattice [33].

---

[3] then known only as the Harper model

[4] It should be noted that Hofstadter himself called it a "recursive structure", for the word "fractal" had been coined by Benoit B. Mandelbrodt [27] only a year prior

It is these transitions that appear in the properties of the eigenstates that are due to phase coherent mechanisms (namely, the interference of a destructive nature). Thus, they serve as ideal testing grounds for decoherence (or protection against it) upon an introduction of noise into the system.

Chapter 3

Model and Implementation

Most of the work carried out as a part of this thesis was computational in nature. The objective of this work was to study the spectral properties and the dynamics of single wavepacket on a tight-binding chain with correlated, time-dependent ($\delta-$pulsed) disorder, and to observe departures from both the static as well as the perfectly periodic case brought about by noise in the kicking.

3.1 Model - Kicked Aubry-André-Harper

The model considered here is a tight-binding chain with a kicked on-site potential. The Hamiltonian is identical to the AAH, except for a δ-kicking of the on-site potentials. It is given by

$$\begin{aligned} H = -J\sum_{i=1}^{L}\left(c_i^{\dagger}c_{i+1}+c_{i+1}^{\dagger}c_i\right)+V\sum_{n}\delta(t-T_n)\sum_{i=1}^{L}V_i c_i^{\dagger}c_i, \\ V_j = \cos(2\pi\alpha j+\phi); \qquad \alpha-\text{Modulation Parameter}, \end{aligned} \tag{3.1}$$

where T_n is the time at which the n^{th} kick is delivered. In the periodic case, $T_n = n\tau$, where τ is the period of the kicking. ϕ is an arbitrary phase which allows a disorder averaging to be performed.

Upon introducing δ-kicking and $\alpha = \frac{\sqrt{5}-1}{2}$[1], it was found that the Metal-Insulator transition described in Section 2.2 persists [7]. The critical kicking strength can now be found in by considering the Floquet operator in a high-frequency, weak-potential expansion. For any generic $H = \hat{H}_0 + \sum_n \delta(t-T_n)\hat{V}$, the Floquet operator can be written as

$$U(\tau^+, 0^+) = e^{-\imath\hat{V}}e^{-\imath\tau\hat{H}_0}, \tag{3.2}$$

---

[1] For the remainder of this thesis, the ‘AAH Model’ will refer solely to the case with this α

where the superscript $+$ indicates the mapping of the system between two instants immediately after kicks. This reduces, in the high-frequency, weak-potential expansion, to

$$\exp\left(-\imath\tau\left\{\hat{H}_0+\frac{1}{\tau}\hat{V}+\dots\right\}\right). \tag{3.3}$$

The effective Hamiltonian $H_{\text{eff}}=\hat{H}_0+\frac{1}{\tau}\hat{V}$ enables one to make the naive guess that the transition occurs at $V/J\tau\sim 2$, corroborated by numerical studies.

In the classical limit, this Hamiltonian exhibits chaotic behaviour, as the kicking eliminates energy as a conserved quantity. This can be seen in the following fashion –

$$\begin{aligned}
&\sum_x |x\rangle\langle x+1| \to \exp(-\imath\hat{p})\\
&\sum_x |x+1\rangle\langle x| \to \exp(\imath\hat{p}).
\end{aligned} \tag{3.4}$$

$$\begin{aligned}
-J\sum_{i=1}^{L}\left(c_i^\dagger c_{i+1}+c_{i+1}^\dagger c_i\right) &= -J\sum_x\left(|x\rangle\langle x+1|+|x+1\rangle\langle x|\right),\\
&= -2J\cos(\hat{p}) \qquad (3.5)\\
\implies H_{\text{cl}} &= -2J\cos(p)+V\sum_n\delta(t-T_n)\cos(2\pi\alpha x). \qquad (3.6)
\end{aligned}$$

This H_{cl} gives rise to the so-called “Kicked Harper map”:

$$\begin{aligned}
p_{n+1} &= p_n+2\pi\alpha V\sin(2\pi\alpha x_n)\\
x_{n+1} &= x_n+2J\tau\sin(p_{n+1}).
\end{aligned} \tag{3.7}$$

Note that this classical map arose out of taking a continuum limit of the kicked tight-binding model. Numerical investigations show that such a model is chaotic regardless of the value of α, leading one to posit that all kicked tight-binding chains ought to be quantum-chaotic. This is yet another ‘1.5 degrees of freedom’ system that displays nonintegrable dynamics. Numerous studies on this map [34–36] have effectively established what is known about the Aubry-André-Harper model to be true even under the presence of kicking, with the addition of intriguing dynamics such as ballistic transport *and* quantum localisation, depending on the location in (semi-classical) phase space [34]. These have been corroborated by studies on their tight-binding analogues which have begun to be explored only recently [7, 37].

3.2 Quantities of Interest

3.2.1 Spectral Properties

Owing to its quantum-chaotic behaviour, it is of interest to study the level statistics of the quantum system, to see if there is a limit in which the generic surmises or conjectures (such as for the level spacing distribution) hold. The quantities of interest, then, are the distributions of the level spacing s and the ratio of consecutive differences r, both of which carry signatures of the integrable-chaotic transition in systems.

Consider a Hamiltonian H with energy levels $\{E_0, E_1, \dots E_N\}$. In order to obtain the universal features of the level distribution, one first has to 'unfold' the spectra [38, 39], such that the local density of states is 1. For this discussion, let $\delta E_i \ll N$ set the scale of locality. δE_i should also be large enough that $\frac{\rho(E)}{N}$ is smooth over the energy scale δE_i. Then, in an interval $[E_i, E_i + \delta E_i)$ with m values, define

$$\begin{aligned} \bar{s} &:= \delta E_i / m \\ \widetilde{E}_i &:= E_i / \bar{s} \\ s_i &= \widetilde{E}_{i+1} - \widetilde{E}_i. \end{aligned} \tag{3.8}$$

The distribution of s is then studied, which is expected to follow the following distributions [40, 41]

$$P(s) = \begin{cases} e^{-s}, & \text{Integrable} \\ A_\beta s^\beta e^{-c_\beta s^2}, & \text{Chaotic, } \beta = 1, 2, 4 \text{ (depending on the symmetries of } H) \end{cases} \tag{3.9}$$

$\beta = 1$ corresponds to the well studied Gaussian Orthogonal Ensemble (GOE) class of random matrices, which describes a system with time-reversal symmetry.

However, such an unfolding process can be far from straightforward, notably in the case of fractal spectra, where a notion of a *smooth* local density of states is hard to define[42]. In such cases, one can instead choose to work with the ratio of consecutive (unfolded) level spacings [43, 44], defined as

$$r_i = \frac{E_{i+2} - E_{i+1}}{E_{i+1} - E_i} \tag{3.10}$$

$$\widetilde{r}_i = \min\left(r_i, \frac{1}{r_i} \right). \tag{3.11}$$

In addition to $P(r)$, $\langle \widetilde{r} \rangle$ is also used to signify the transition between Poisson (~ 0.386) and GOE

(~ 0.536) statistics [43].

In Floquet systems, however, there is no meaning to defining a spectrum as described above. However, it is found that many of the Random Matrix Theory predictions hold instead for the eigenvalues ε_a of the Floquet Hamiltonian of Eq. (2.4). In practice however, especially for δ-kicked systems which have Floquet operators of the form given in Eq. (3.2) and are thus directly computable, one simply diagonalises $U(\tau^+, 0^+)$, and extracts the phases of the unimodular eigenvalues. Identical procedures are carried out, with a caveat. Accordance with the corresponding unitary ensembles implies that one should not have to unfold the spectra, because all unitary ensembles have universally uniform level spacing distributions. However, unfolding might still have to be done if the peculiarities of the Floquet operator lead to a high density of states in certain regions; after all, the universal features regard only the fluctuations.

Over the course of this work, the distributions of both s and r were calculated for the AAH Model, in the delocalised, localised and critical phases, wherein difficulties with unfolding were manifest in the latter case.

3.2.2 Dynamics

This project also involved the study of the dynamics of a wavepacket initially localised at the center of the chain. The dynamics on the chain is characterised by two quantities – the spread of a wavefunction initially localised at the center of the lattice $\sigma^2(t)$and an instantaneous, locally averaged diffusion exponent γ_m, both defined below.

$$\sigma^2(t) = \sum_{i=1}^{N} (i - N/2)^2 |C_i(t)|^2; \; C_i(t) \equiv \langle x_i | \psi(t) \rangle \tag{3.12}$$

$$\gamma_m(t) \equiv \frac{1}{m} \sum_{\bar{t}=-\frac{m}{2}}^{\frac{m}{2}}{}' \frac{\log\left(\sigma^2\left(t+\bar{t}\right)\right) - \log\left(\sigma^2(t)\right)}{\log\left(1+\frac{\bar{t}}{t}\right)} \tag{3.13}$$

γ_m is also complemented by fits of σ; its utility, however, lies in its ability to obtain local variations in the dynamics. The caveat, then, is that genuine local fluctuations need to be aptly distinguished from noise, especially in the cases where the system is aperiodically driven.

Building on previous work on this model [7, 37], stochasticity is introduced in the kicking, either in the strength, the period or in both. Several protocols inspired largely by previous studies on the kicked rotor [13, 14] were implemented. These are tabulated in Table 3.1.

Previously held notions on noisily driven quantum systems were that decoherence is to be generically expected, with coherence lost at an exponential rate[9, 12, 45]. Recent work, however,

Type of Noise	Description
(A) Timing (Aperiodicity) [37]	The spacing between consecutive kicks is a uniform random number drawn from the interval $[T-\delta T, T+\delta T]$
(B) Timing (Missed) [14]	The spacing between kicks is in itself a random number drawn from the uniform, normal and poisson distributions
(C) Amplitude & Timing [13]	Kicks are delivered periodically, but at a randomly chosen time, the amplitude V is altered by a random amount δV

Table 3.1: Descriptions of various schemes

has showed that this need not be the case [13, 14]. In order to establish if the phenomena here are due to phase-coherent effects, the evolution of noise-averaged Fidelity $\mathscr{F}$ defined as

$$\begin{aligned} \overline{\mathscr{F}(t)} &:= \operatorname{Tr}\rho^2(t) \\ \text{where } \rho(t) &= \overline{|\psi(t)\rangle\langle\psi(t)|}, \end{aligned} \tag{3.14}$$

has also been calculated.

3.3 Technical Details and Implementation

The numerical work was implemented in C++ using the Armadillo linear algebra library [46, 47], aided by Intel®'s Math Kernel Library [48]. In order to obtain the level statistics, the Floquet operator (Eq. (3.2)) was exactly diagonalised, and the consequent differences between the eigenphases were considered.

The dynamics was studied by choosing an initial wavefunction on a lattice of size N such that $\langle x|\psi(t=0)\rangle = \delta_{x,N/2}$. At every time step it was acted open by the unitary operator $e^{-\imath\tau\hat{H}_0}$; $\hat{H}_0 = -J\sum_{i=1}^{L}\left(c_i^\dagger c_{i+1} + c_{i+1}^\dagger c_i\right)$, with a kick $e^{-\imath\tau V}$; $\hat{V} = V\sum_{i=1}^{L}\cos\left(2\pi\alpha j+\phi\right)c_j^\dagger c_j$ applied at times T_n. The difference between successive kicks $T_{n+1}-T_n \equiv k\tau$, where k was a random integer drawn from different distributions. The case where the application of $e^{-\imath\tau\hat{V}}$ depends on the result of a coin-toss with variable bias has also been studied. These are all implemented by direct matrix multiplication, since $\hat{H}_0$ is tridiagonal in the position basis, and can be efficiently diagonalised and hence, exponentiated.

The code used over the course of this project is provided in the Appendix.

Chapter 4

Results and Discussion

The results of extensive numerical simulations form the crux of this section. First, level statistics – specifically, of level spacing ratios, for the kicked model, and compare them against those of the static model. Then, the results for the dynamics are presented, following which the outcome of some analysis (fits and the calculation of γ_m) is shown, with some exact results. The highlight is that many of the observations in the AAH model seem not to depend on the breaking of translational invariance.

4.1 Level Statistics

To reiterate, the level spacing ratios r_i are defined, as in Eq. (3.10), as

$$r_i = \frac{E_{i+1} - E_i}{E_i - E_{i-1}},$$

where the E_i refer to the unfolded levels in the spectrum. Figure 4.1 shows the distribution of r for the cases where the onsite potentials resembling the AAH and the Anderson (uncorrelated disorder) model are kicked periodically. In the AAH model, the delocalised regime shows level repulsion, but it does not ascribe to any standard random matrix class of quantities[1]. Note that there are no effects of the density of states in this case, since the ratios are robust in that sense to finer details.

The localised phase, on the other hand, shows remarkable regularity in the level spacing distribution. There are 3 peaks, roughly at 0.6, 1 and 1.6 $\left(\sim \frac{1}{0.6}\right)$. While the generic expectation for integrable/localised systems is $P(r) = \frac{1}{(1+r)^2}$, this does not necessarily hold for 1-D, 1 particle

---

[1] These are NOT the same as Eq. (3.9), which pertained to level *spacing* distribution

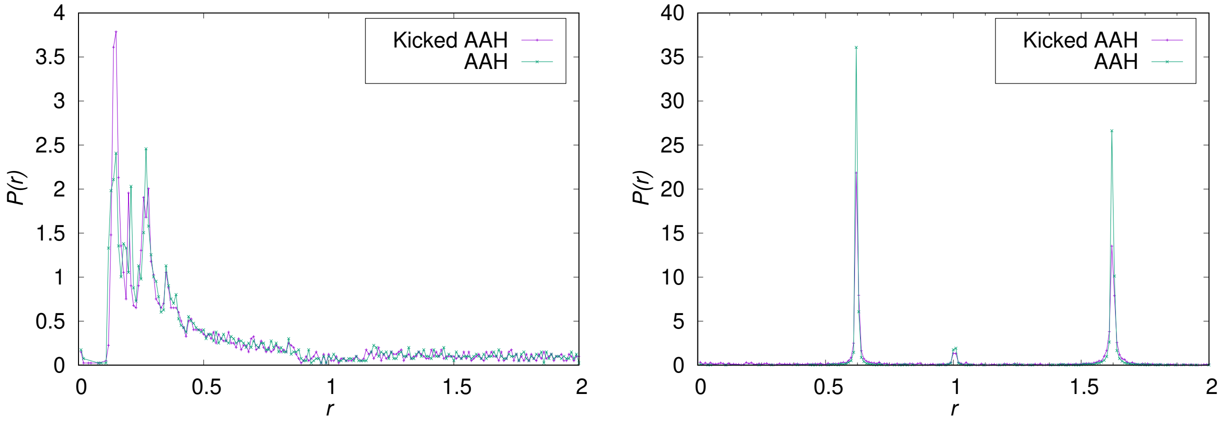

(a) Delocalised phase

(b) Localised phase

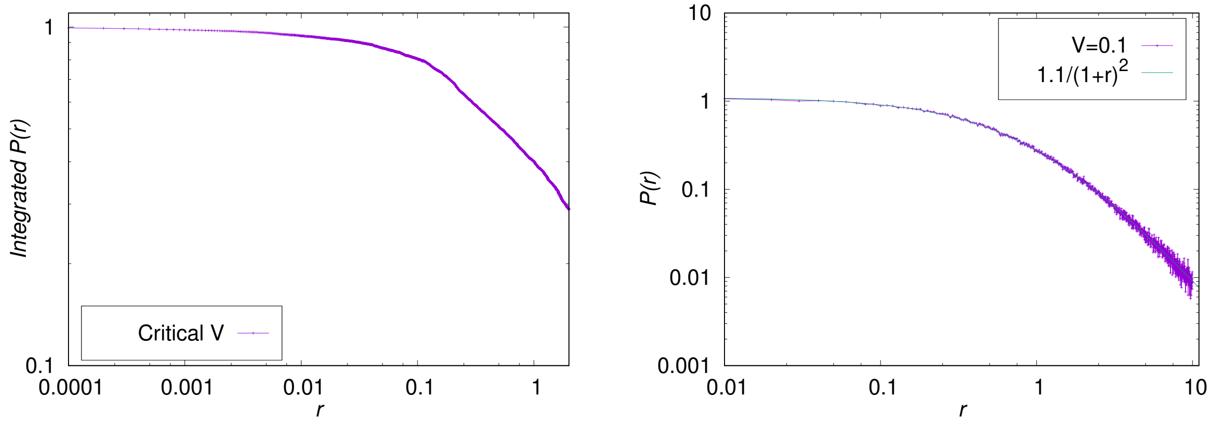

(c) Integrated distribution for the critical case

(d) Anderson Model, $V = 0.1$

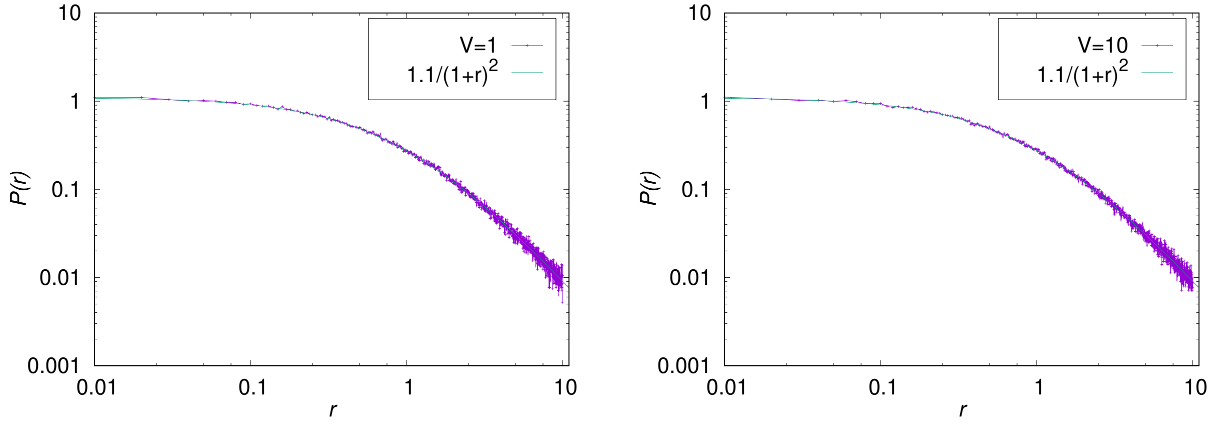

(e) Anderson Model, $V = 1$

(f) Anderson Model, $V = 10$

Figure 4.1: Distribution of level spacing ratio r for the kicked system (shown in purple). Those of the static case are shown in green

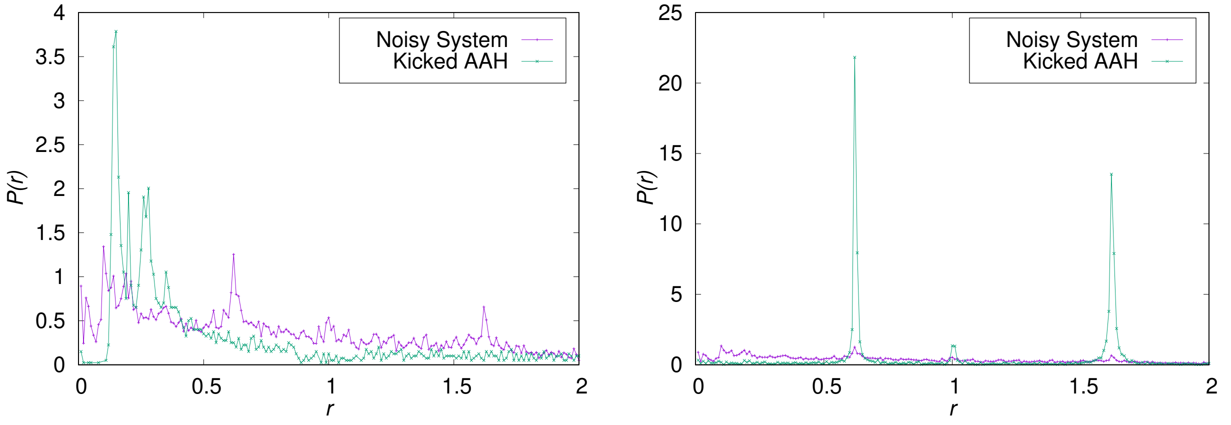

(a) Delocalised regime, after 7 kicks

(b) Localised regime, after 7 kicks

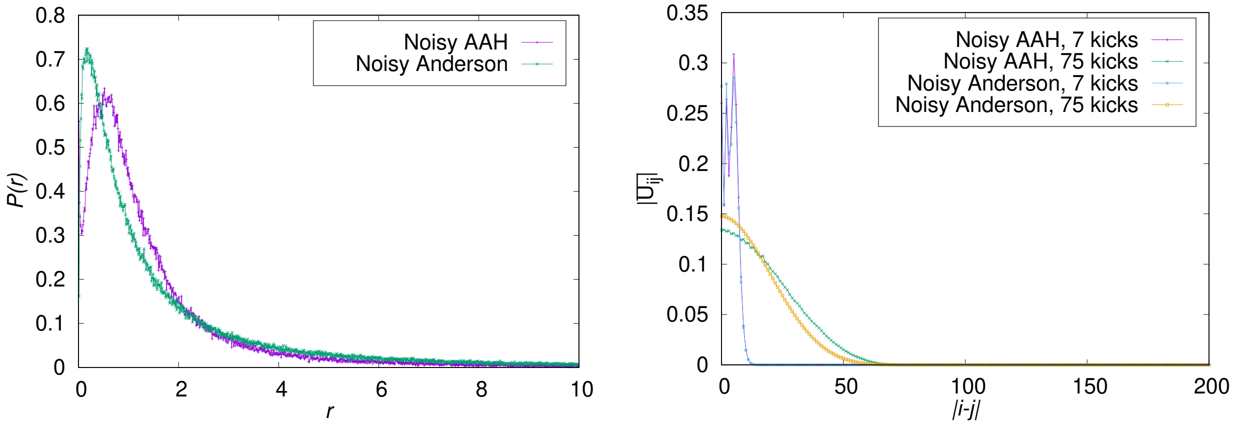

(c) At late times

(d) $\overline{|U_{ij}|}$ vs $|i-j|$ for early and late times

Figure 4.2: Statistical properties of the (noisy) evolution operator

Hamiltonians. It's easy to see, that in addition to the possibility of widespread degeneracy/level clustering, systems adhering to those conditions also exhibit evenly spaced levels which would thereby cause peaks at $r = 1$[2]. The peaks at $r = 0.6, \sim \frac{1}{0.6}$ suggest the existence of two levels with uniform, identical spacing superimposed on one another with some staggering or levels with alternating differences. Employing and adapting methods that have since been developed [49], one can attempt to understand if such a result is genuinely caused by the overlap of two such spectra and thus, if there is an emergence of a new symmetry. The Anderson model, on the other hand, shows near-perfect adherence to the ansatz $P(r) = \frac{1}{(1+r)^2}$ regardless of kicking strength.

The level distributions of the noisy evolution operator, averaged over several iterations, begin showing deviations from the periodically kicked model quite early. In the graphs of Fig. 4.2,

---

[2] Think simple harmonic oscillator

(de)localised means that the kicking term is in those respective regimes. At late times, the distributions flatten out into smooth curves that exhibit level repulsion, in line with the observation of diffusion at large times.

The distribution of matrix elements as a function of their distance from the diagonal has been calculated for the case where the kick times are drawn uniformly from $[1,10]$, averaged over each matrix of each iteration. The "early" time has been chosen to be 7 kicks because it takes a few kicks to obtain a form qualitatively different from that of the free limit, and not longer because there is a sharp break in the dynamics around $t/\tau \sim 10$, to be shown in Chapter 4. By $t/\tau = 75$, the system has reached its asymptotic behaviour.

4.2 Dynamics

The study of the dynamics involves the calculation of $\sigma^2(t)$ as in Eq. (3.12). In all cases, $\langle x|\psi(t=0)\rangle = \delta_{x,\frac{L}{2}}$, where L is the size of the lattice, $\tau = 0.5$ and $J = 1$, resulting in $V_{\text{critical}} \sim 2J\tau = 1$. The graphs that show the dynamics of σ^2 also have, as a guide, the curves $\left(\frac{t}{\tau}\right)^\gamma$ for $\gamma = 1,2$, indicating diffusive and ballistic growth, respectively.

4.2.1 AAH Model

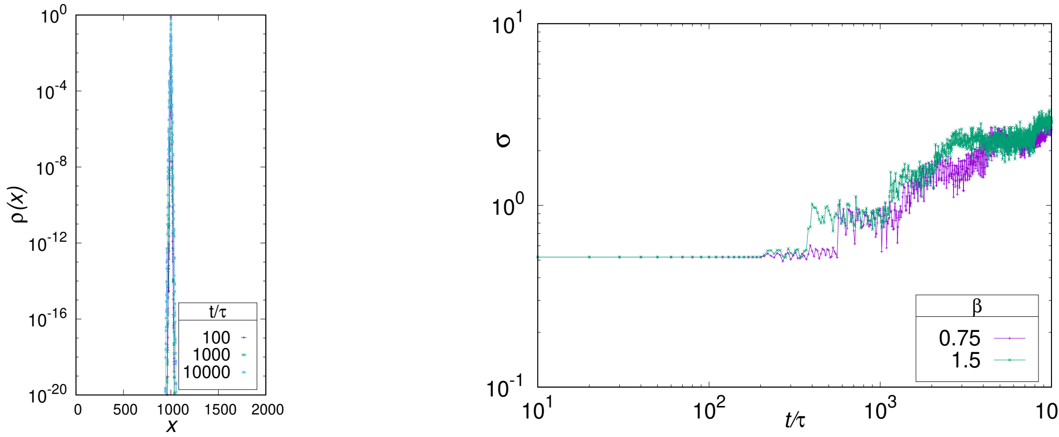

Figure 4.3: Density profile ($\beta = 0.75$) and spread of the wavefunction for protocol (C), where timing noise is drawn from a Yule-Simon distribution with exponent β and amplitude noise uniformly from $[-V/2, V/2]$

Figure 4.3 follows Protocol (C) in Table 3.1, where the timing noise is chosen from a Yule-

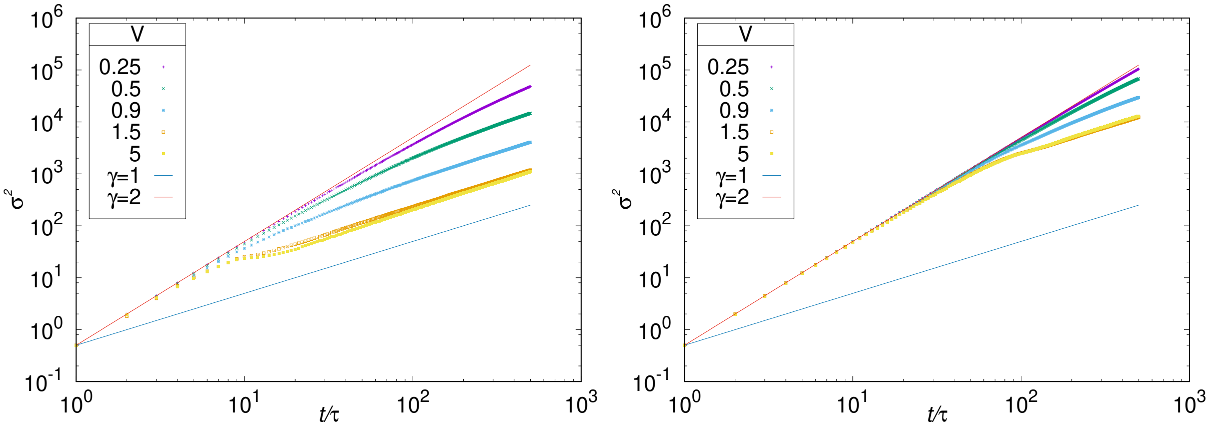

(a) $A = 10$ (b) $A = 100$

Figure 4.4: σ^2 vs. t/τ at $A = 10, 100$ for uniform noise

Simon distribution, given by

$$p(t;\beta) = \beta \frac{\Gamma(t)\Gamma(\beta+1)}{\Gamma(t+\beta+1)}. \tag{4.1}$$

For large t, $p(t;\beta) \sim t^{-(\beta+1)}$. The amplitude noise δV is drawn uniformly from $[-V/2, V/2]$. Even for such a strong perturbation, it is found that localisation persists. Since similar results are found for the case where the timing noise is uniformly distributed, and for Protocol (A) [37], the underlying cause for this robustness might be a question worth exploring. Alternatively, in this thesis, attempts were made to find a way to force the extenuation of localisation, and delivered the following results. Protocol (B) in Table 3.1 is followed for the remainder of this section.

Figures 4.4 and 4.5 describe the results where the times between kicks is drawn from a uniform integer distribution. It can be seen from the graphs that for V above a certain threshold, a sharp break in the dynamics appears. The break occurs between an initial ballistic/superdiffusive dynamics that can be made to last arbitrarily long and diffusive dynamics, which persists as $t \to \infty$. What is more striking is that, for kick times drawn uniformly from $[1, A]$, the break appears to occur almost exactly at $t/\tau = A$ or in a very small neighbourhood around it. Figure 4.4 exhibits that for V above a certain limit that the break time occurs at $A = 10, 100$ respectively. Figure 4.5 shows that the limit is none other than the critical limit $V = 1$. It appears that once the driving is well in the localised limit, it matters only that the eigenstates are localised, as the dynamics for $V \geq 1.5$ mimic each other exactly, while a range of initial time difffusive exponents can be seen for $V < 1$. Analogous to the metal-insulator transition, it appears as though the sharpness builds as

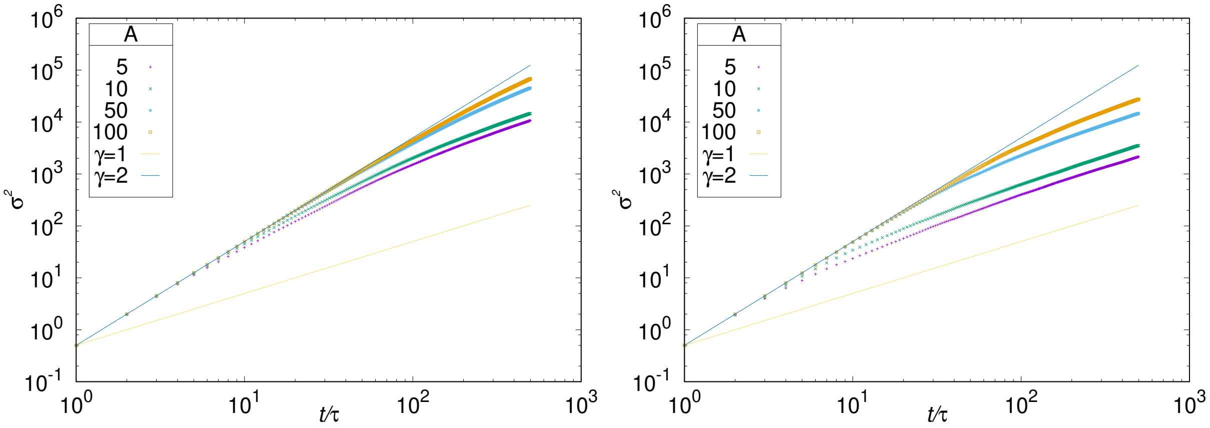

(a) $V = 0.5$ (b) $V = 0.95$

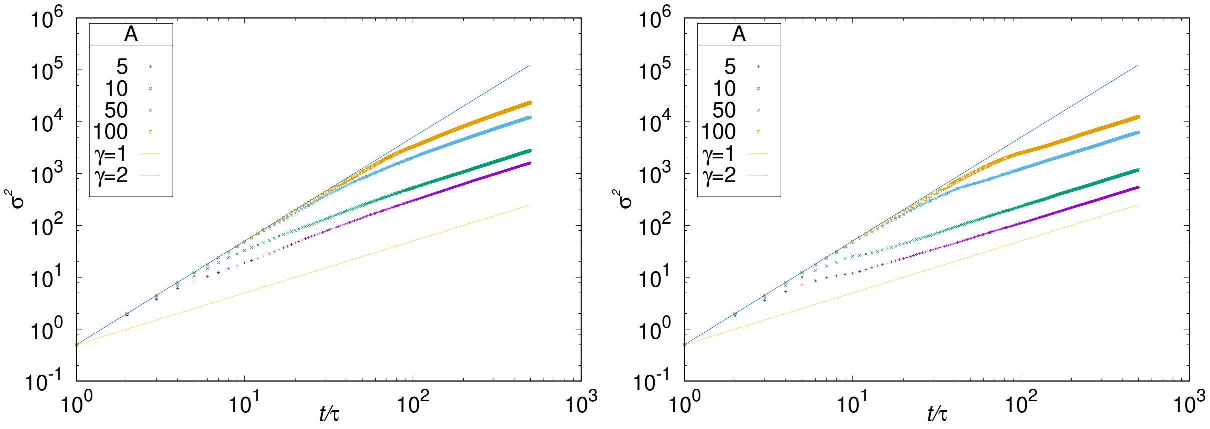

(c) $V = 1.05$ (d) $V = 1.5$

Figure 4.5: σ^2 vs. t/τ for kick times drawn from $[1, \mathrm{A}]$ at $V = 0.5, 0.95, 1.05, 1.5$

V is increased, wherein, after $V = 1$, the sharpness becomes well-defined and evident.

Figures 4.6 and 4.7 exhibit much the same results, where the time between kicks is drawn from a Poisson distribution instead. The crucial factor of the distribution of which advantage has been taken is the ability to vary the mean waiting time λ *continuously*, in contrast to the tunable parameter in the case of uniform noise. This brings to light 3 different types of dynamics, which can be tuned solely by varying λ.

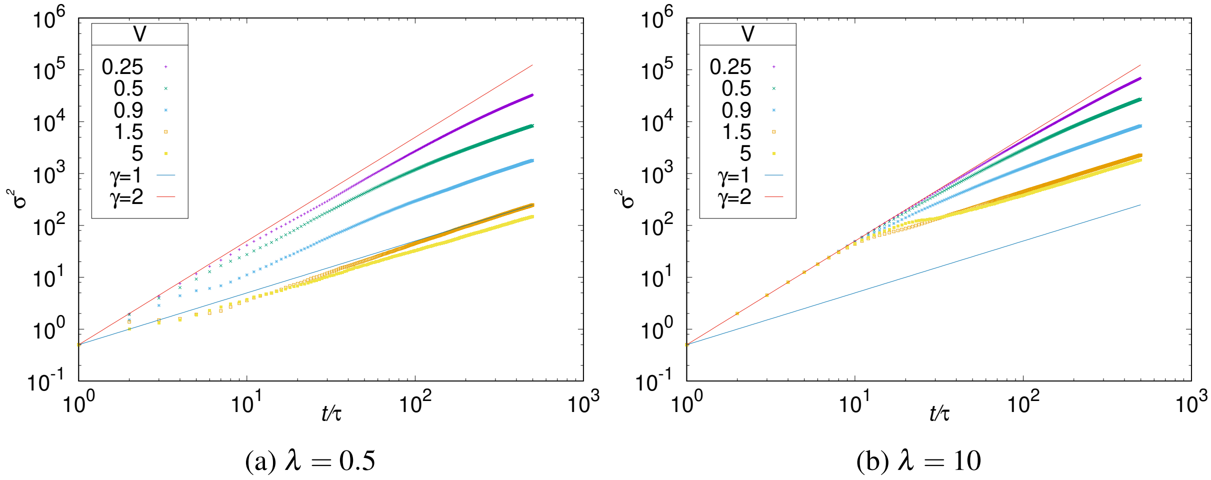

(a) $\lambda = 0.5$ (b) $\lambda = 10$

Figure 4.6: σ^2 vs. t/τ at $\lambda = 0.5, 10$ for Poisson noise

For very small λ, there is period of transient shuffling following which the dynamics of the periodically kicked Hamiltonian is followed, until diffusion sets in at much longer times (longer when $V < 1$ than when $V > 1$). Consider the cases where $V < 1$. For intermediate λ, there is a transient dynamics which preceeds an intermediate time where the spread is faster than the transient, until there is a gradual crossover to diffusion from superdiffusive dynamics. At large $\lambda > 2$, there is an initial superdiffusive/ballistic growth which again, gradually crosses over to diffusion, as in the case of uniform noise. When $V > 1$, however, the sharp break between superdiffusive and diffusive growth emerges. For λ intermediate, where there are 3 distinct temporal regimes, a borderline case where the dynamics is diffusive from the start arises, again as $\lambda \sim 2$. After this, the initial dynamics becomes faster (until its diffusion exponent $\gamma = 2$) and persists for longer, with a sharp break to diffusive dynamics.

Similar results are observed in cases where the time between kicks is taken to be $1 + x$, where x is the integer part of Gaussian distributed variable, restricted to take positive values, with standard deviation β. The exception here is that the mimicing of the periodically driven dynamics for small β appears to persist for much longer than in the Poisson case[3]. These results are shown in Figs. 4.8

---

[3] The substantiation of this point requires a more apposite means of comparison between the different types of noise

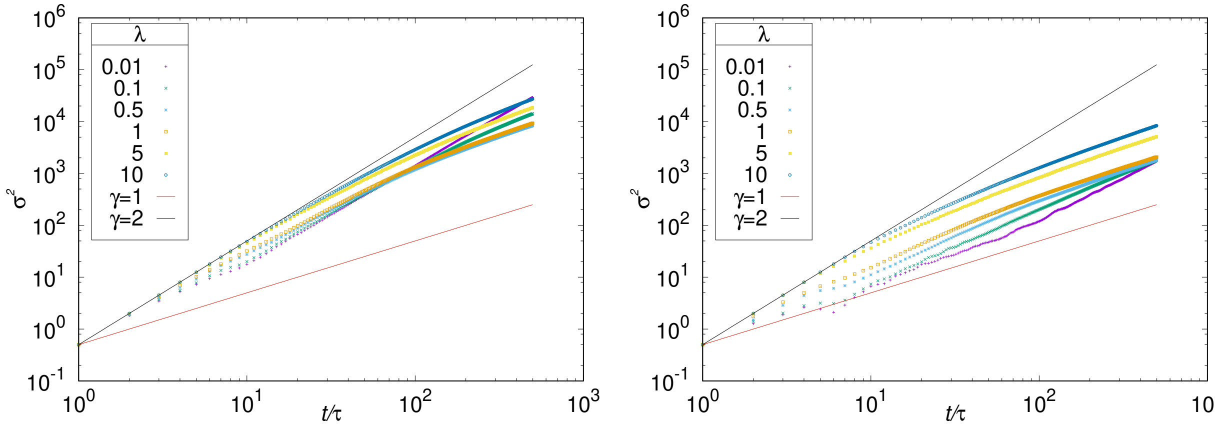

(a) $V = 0.5$

(b) $V = 0.9$

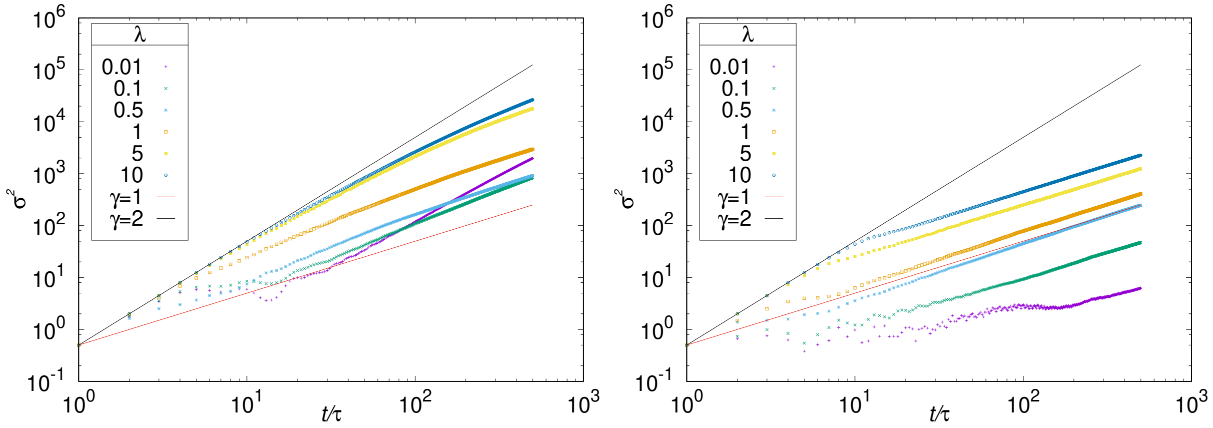

(c) $V = 1.1$

(d) $V = 1.5$

Figure 4.7: σ^2 vs. t/τ for Poisson kick times, with mean waiting λ at $V = 0.5, 0.9, 1.1, 1.5$

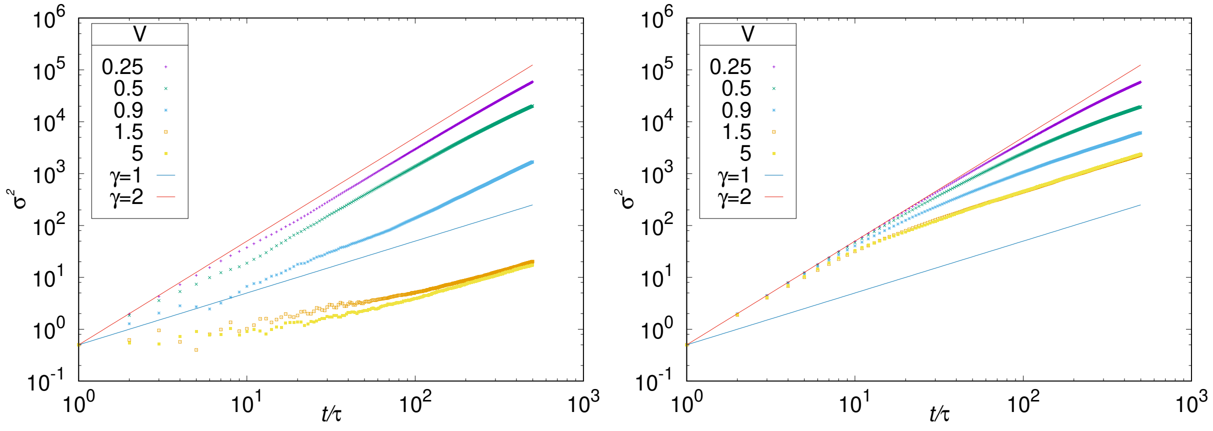

(a) $\beta = 0.5$

(b) $\beta = 10$

Figure 4.8: σ^2 vs. t/τ at $\beta = 0.5, 10$ for Normal noise

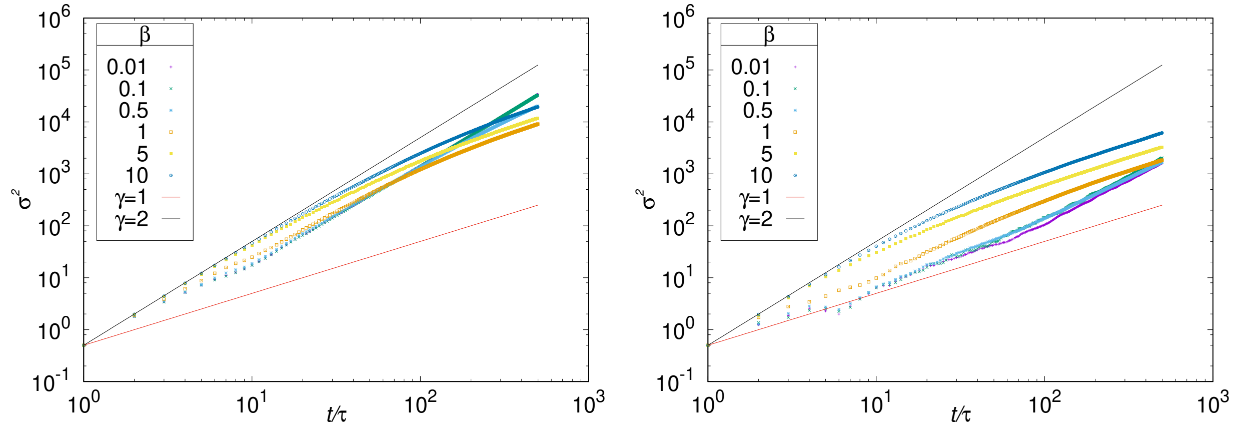

(a) $V = 0.5$ (b) $V = 0.9$

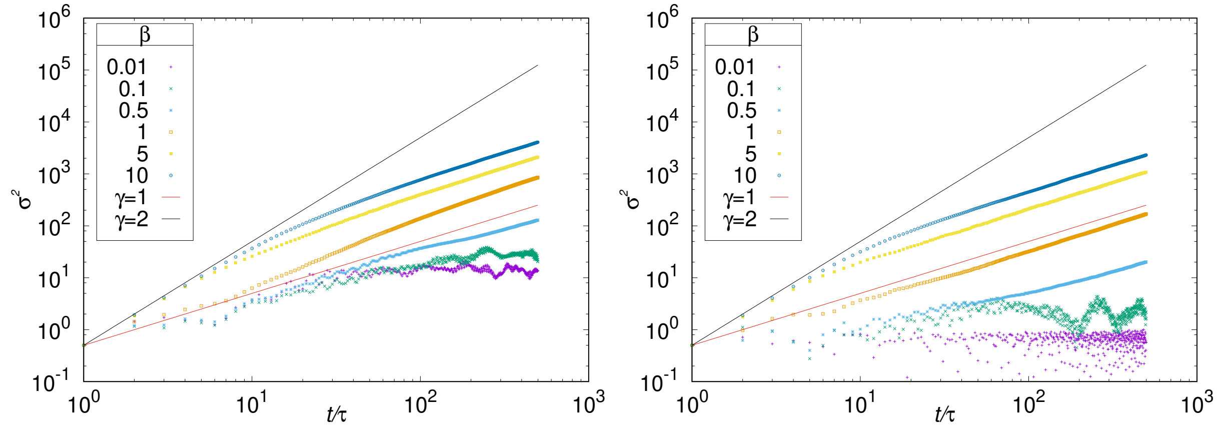

(c) $V = 1.1$ (d) $V = 1.5$

Figure 4.9: σ^2 vs. t/τ for Normal kick times with standard deviation β at $V = 0.5, 0.9, 1.1, 1.5$

and 4.9.

---

and their relevance to this system

4.2.2 Translationally Invariant Models

In the preceeding section, the only universal feature across all values of V was the long-term diffusive limit of the dynamics. Crucially, the sharp breaking in dynamics appeared to repose on the condition of localisation; of the kicking drastically altering the "free" evolution. Thus, it might be pertinent to explore the role of quasiperiodicity in shaping the dynamics of the system. It is in these cases that the parameter α is tuned, from rational to irrational. A standard way to do this is to consider a sequence S_α such that $\alpha_i = F_i/F_{i+1}$, where F_i is the i^{th} Fibonacci number. Then $\lim\limits_{i\to\infty} \alpha_i = \frac{\sqrt{5}-1}{2}$. However, interesting results begin revealing themselves far in advance of this eventual limit. It is found that the break in dynamics persists even in translationally invariant models! Seeing as how the system is switched between a 1-band model and an m-band model, where m is a small integer, it is surprising to observe a sharp break connecting the two regimes;

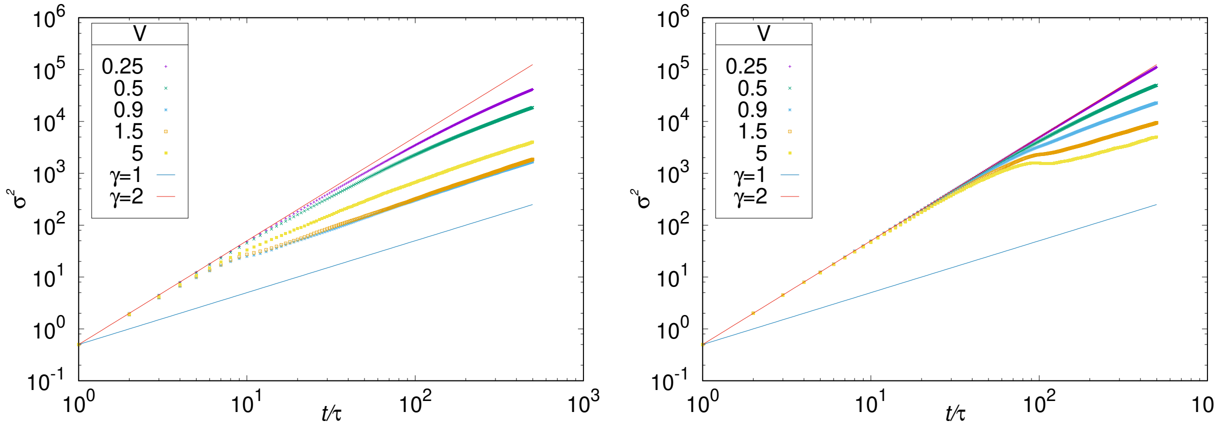

(a) $A = 10$, 2-band model

(b) $A = 100$, 2-band model

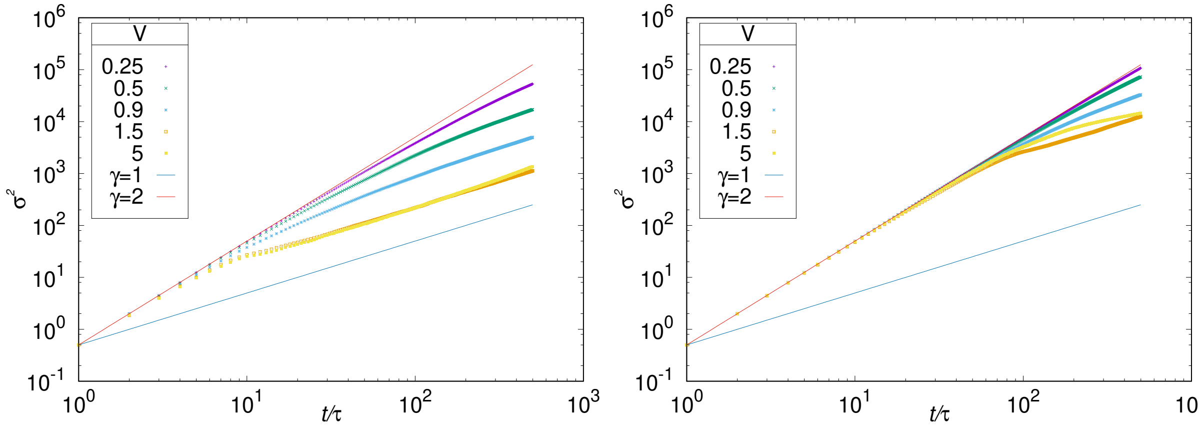

(c) $A = 10$, 3-band model

(d) $A = 100$, 3-band model

Figure 4.10: σ^2 vs. t/τ at $A = 10, 100$ for 2, 3-band models

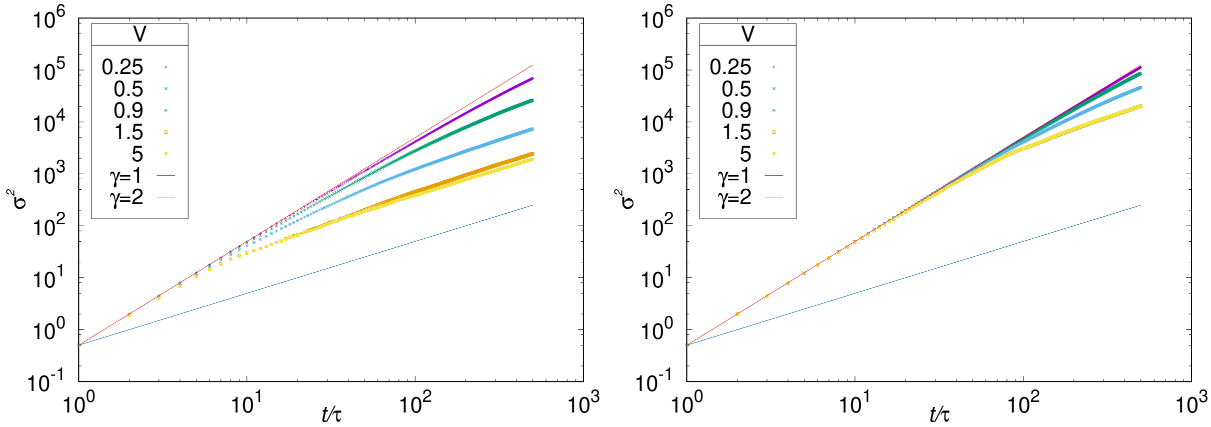

(e) $A = 10$

(f) $A = 100$

Figure 4.10: σ^2 vs. t/τ at $A = 10, 100$ for a 4-band model

the asymptotic can be explained by decoherence. Such dynamics is seen across all the m-band structures simulated, $2 < m < 10$. Figures 4.10 to 4.12 show the presence of these phenomena in the case of uniformly distributed noise in the kick times, while Figs. 4.13 and 4.14 present the cases of poisson distributed noise.

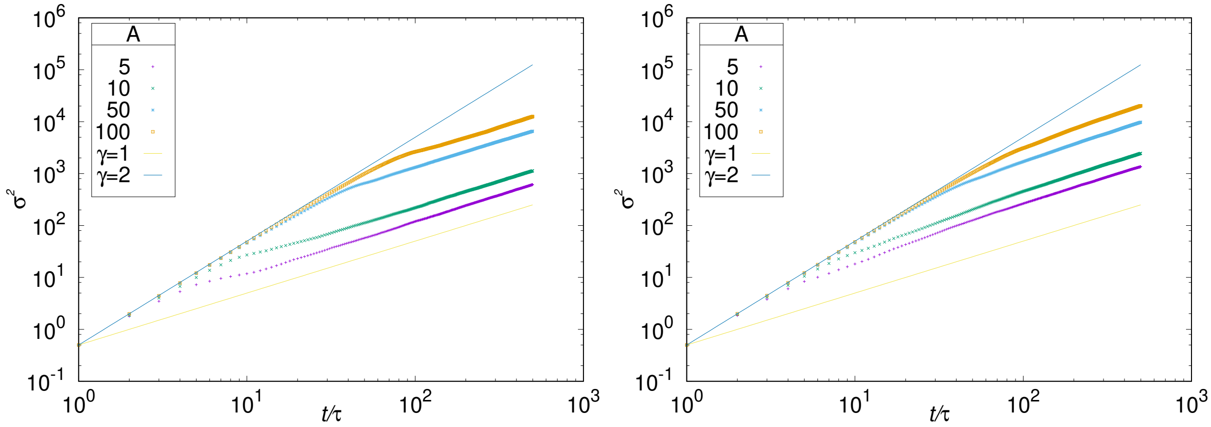

(a) 3-band model

(b) 4-band model

Figure 4.11: σ^2 vs. t/τ at $V = 1.5$ for a 3, 4-band model

Moreover, the absence of a transition point begs the question of the nature of the threshold that determines whether a break is observed. It is also observed that at certain windows of V, there is a drastic slowing down at the break-time of the dynamics, with the diffusion exponent almost reaching zero. A closer look at the band structures is warranted, to determine if there is any obvious change in the structure at these values of V. These are plotted in Figs. 4.15 to 4.17.

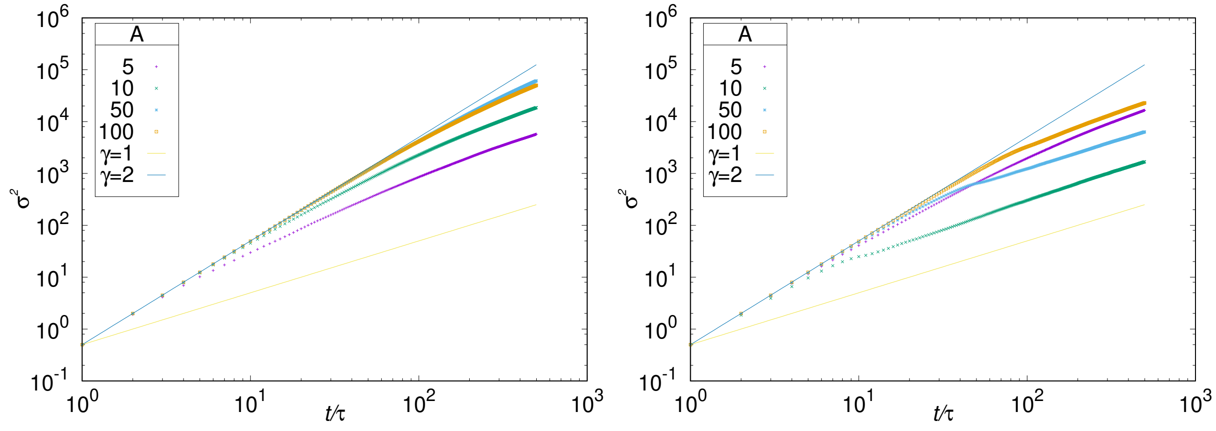

(a) $V = 0.5$

(b) $V = 0.9$

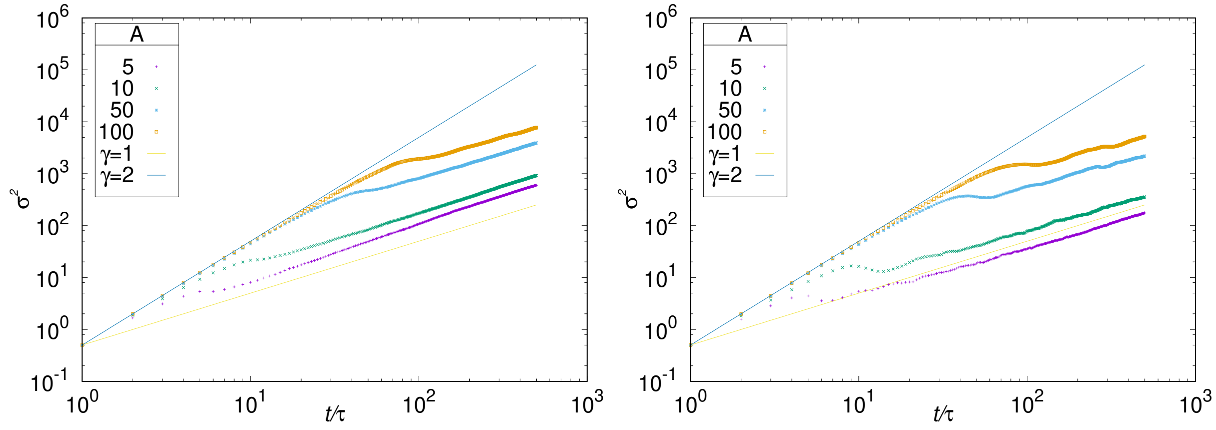

(c) $V = 1.1$

(d) $V = 1.5$

Figure 4.12: σ^2 vs. t/τ for kick times drawn from $[1, \mathrm{A}]$ for a 2-band model

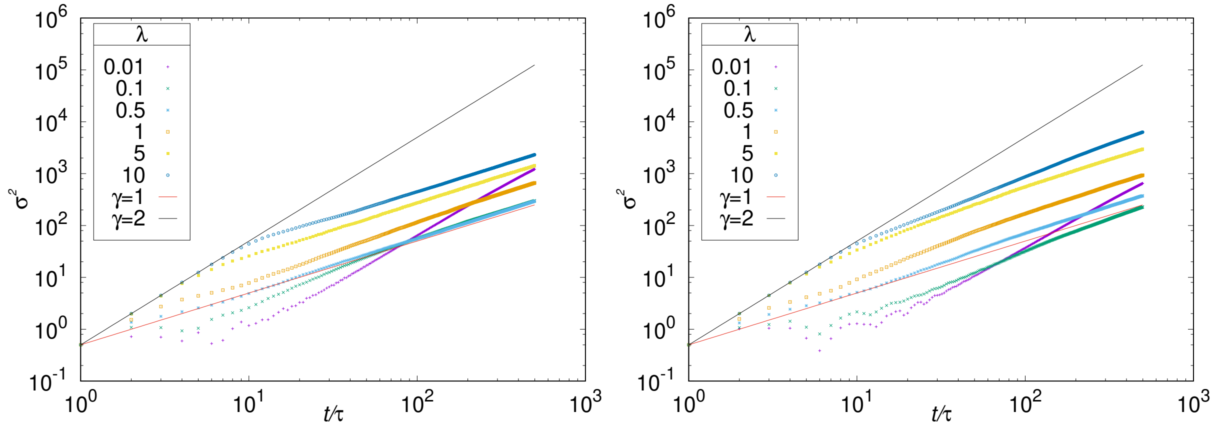

(a) 3-band model

(b) 4-band model

Figure 4.13: σ^2 vs. t/τ at $V = 1.5$ for 3, 4-band models for Poisson noise

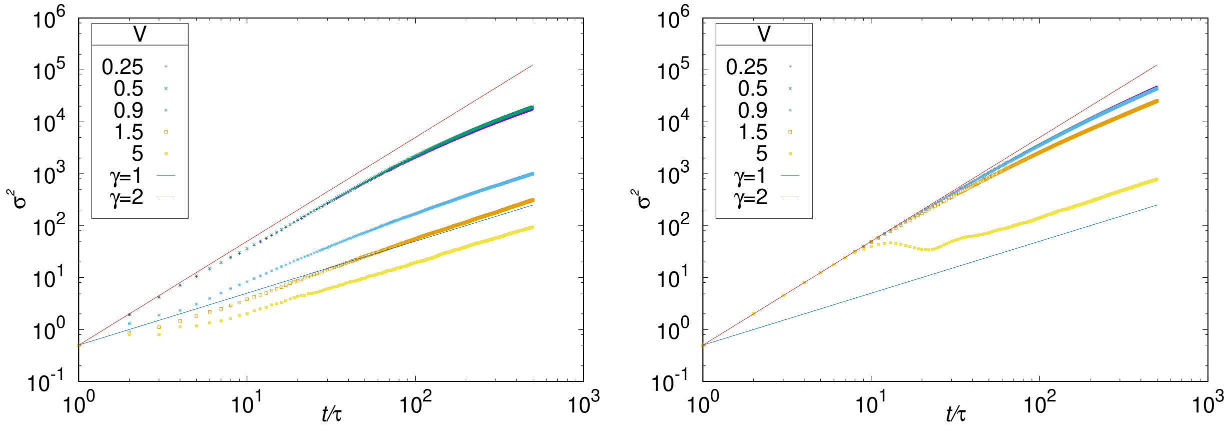

(a) $\lambda = 0.5$, 2-band model

(b) $\lambda = 10$, 2-band model

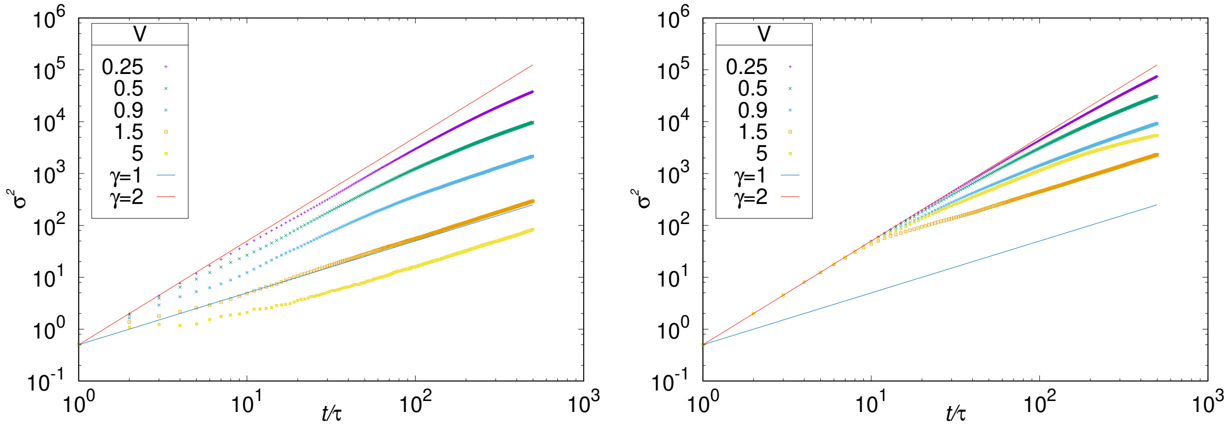

(c) $\lambda = 0.5$, 3-band model

(d) $\lambda = 10$, 3-band model

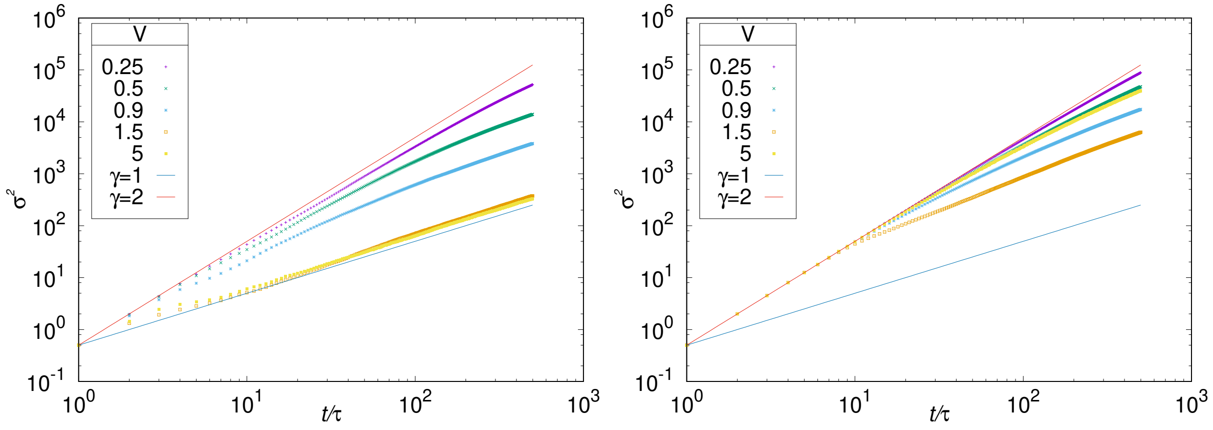

(e) $\lambda = 0.5$, 4-band model

(f) $\lambda = 10$, 4-band model

Figure 4.14: σ^2 vs. t/τ at $\lambda = 0.5, 10$ for 2, 3, 4-band models with Poisson noise

Band Structures

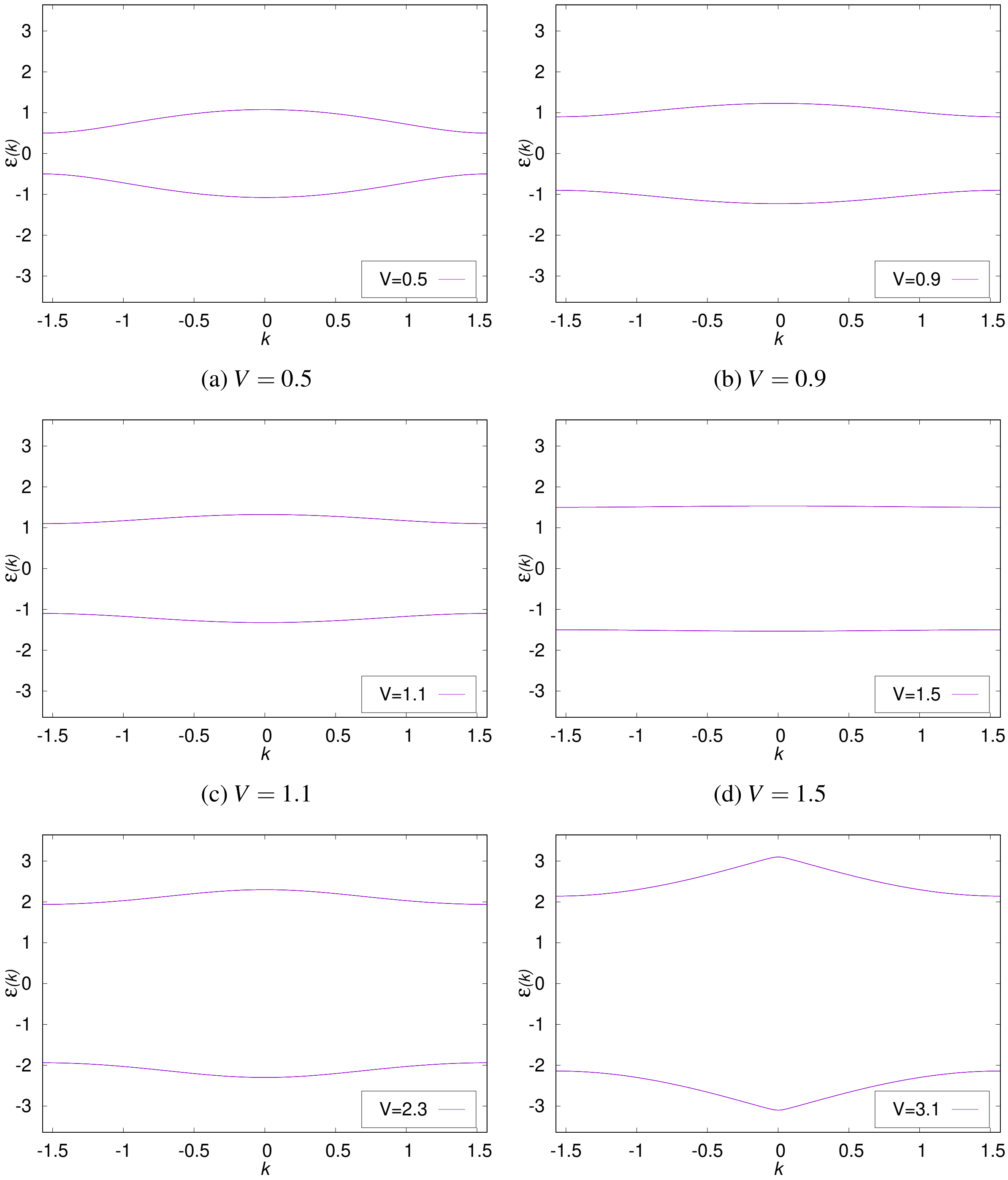

(a) $V = 0.5$ (b) $V = 0.9$

(c) $V = 1.1$ (d) $V = 1.5$

(e) $V = 2.3$ (f) $V = 3.1$

Figure 4.15: Band structures for the 2-band model

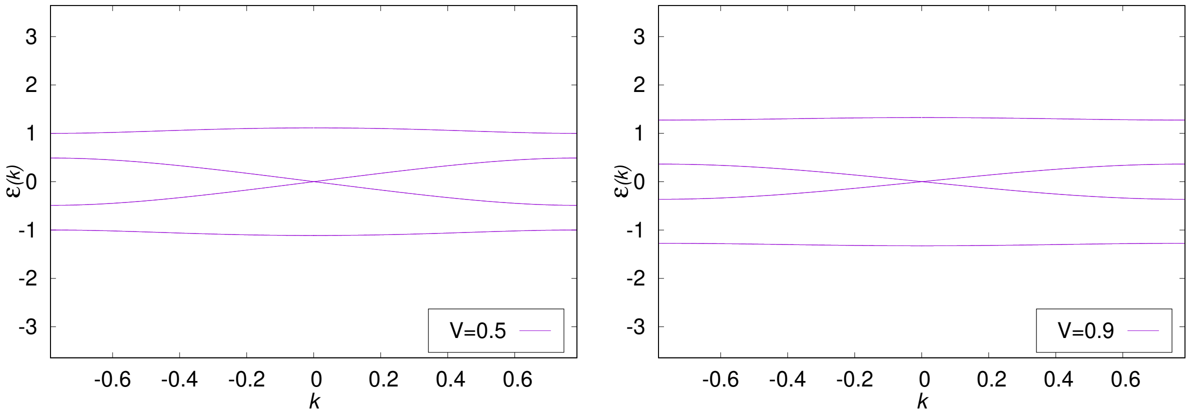

(a) $V = 0.5$ (b) $V = 0.9$

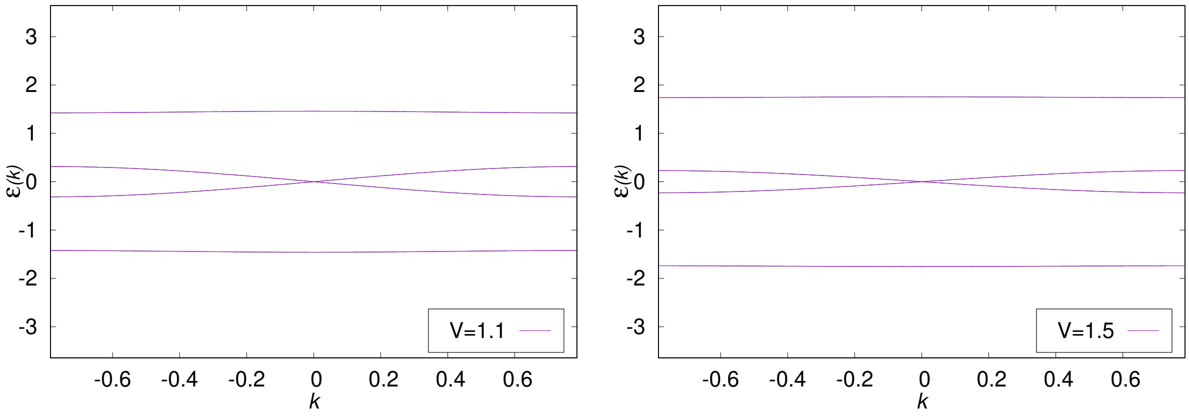

(c) $V = 1.1$ (d) $V = 1.5$

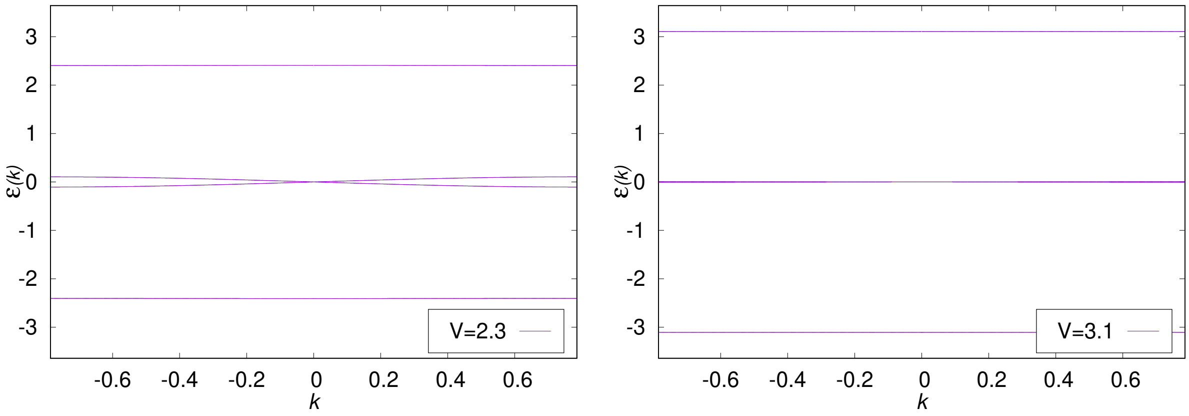

(e) $V = 2.3$ (f) $V = 3.1$

Figure 4.16: Band structures for the 4-band model

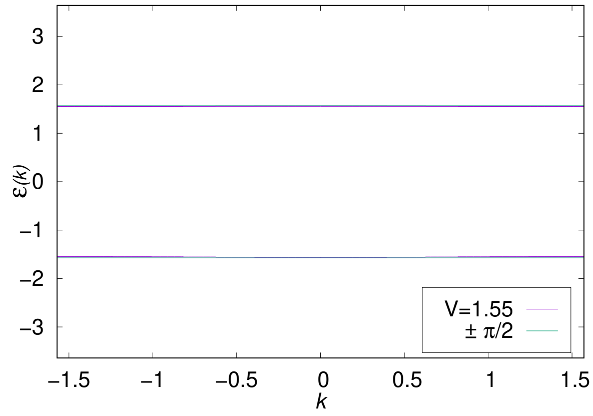

Figure 4.17: Special case of flat bands

The first result that can be observed from the band structures is that the model with kicking alone can be used to engineer flat-bands and hence, the localisation of excitations. This result shall be elaborated upon, presently.

The effective Hamiltonian which gives rise to the same dynamics of the periodic driving over one period can be expanded using a Baker-Campbell-Hausdorff (BCH) expansion, as has been done in Eq. (3.3). In a naïve weak-potential, high-frequency term, one simply obtains again a tight-binding model, with the potential rescaled by τ. However, for no finite strength can there be flat bands in static m-band tight-binding models. Analytically, this can be seen from the simple cases of the 2, 3 and 4 band models. Concretely, the dispersion relation for a 2 band model with onsite potentials $\pm V$ is given by [22]

$$\varepsilon(k) = \pm\sqrt{V^2 + 4J^2\cos^2\left(\frac{ka}{2}\right)}, \tag{4.2}$$

where a is the lattice spacing, and J is the hopping amplitude. Only in the limit where the hopping is completely suppressed and there are on-site terms alone, is the spectrum flat.

But this is not the case for the kicked tight-binding model, as has been seen in Figs. 4.15 and 4.17 for the 2 band model, and in Fig. 4.16 for the 4 band model. It can be shown analytically, by diagonalising the Floquet operator in the 2×2 k-subspaces to give

$$F_k(\lambda) = \begin{pmatrix} \exp(\imath 2JT\cos(k))\cos(\lambda) & -\imath\sin(\lambda)\exp(\imath 2JT\cos(k)) \\ -\imath\sin(\lambda)\exp(-\imath 2JT\cos(k)) & \exp(-\imath 2JT\cos(k))\cos(\lambda) \end{pmatrix}; \tag{4.3}$$

$$\varepsilon(k) = \pm\cos^{-1}\left(\cos\left(2J\tau\cos(k)\right)\cos\left(\lambda\right)\right). \tag{4.4}$$

Thus, the kicking has shown a relatively straightforward mechanism to construct flat bands.

The second – related – result pertains to the onset of the break in dynamics as seen in Figs. 4.10 to 4.12. Upon comparison with the complementary band structures, it is evident that one does not require perfectly flat bands in order to effect either the break or the slowing down in the dynamics at those times, so how "flat" is "flat enough"? Moreover, are there other transitions that one can expect to observe that accompany the appearance of a break in the dynamics?

4.2.3 Fidelity

As stated in the Introduction, one of the quantities of interest in models that show subdiffusion as a departure from localisation, amongst many other models, when subject to noise, is that of Fidelity. The Fidelity obeys the bound $\frac{1}{L} \leq \mathscr{F} \leq 1$ where L is the size of the Hilbert space under consideration. It saturates this bound from above when the density matrix ρ described by the state is pure, and achieves its lower bound when ρ describes a completely statistical mixture (i.e. devoid of coherence). In this subsection, the results of Fidelity calculations for uniform and poisson noise in the kicking with $\alpha = \frac{\sqrt{5}-1}{2}$ are shown.

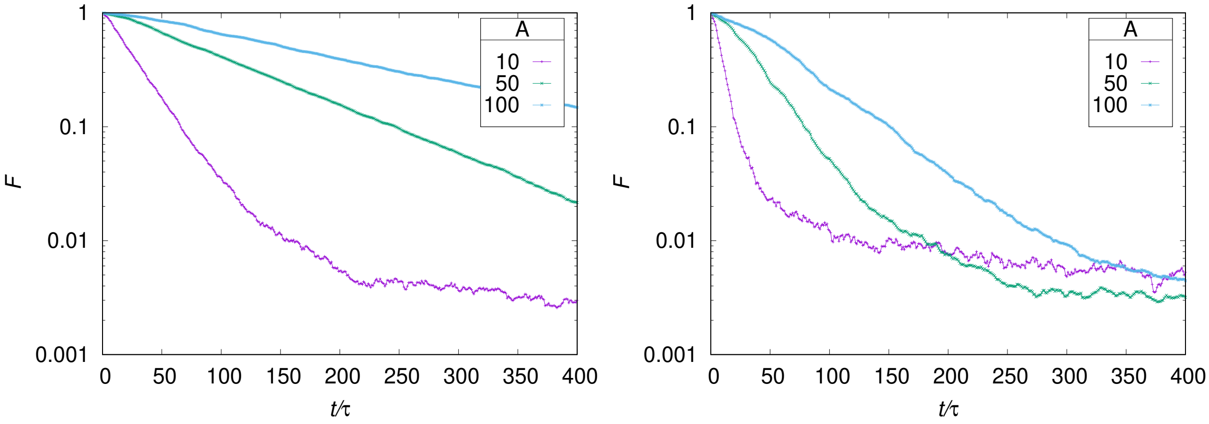

(a) $V = 0.5$ (b) $V = 0.9$

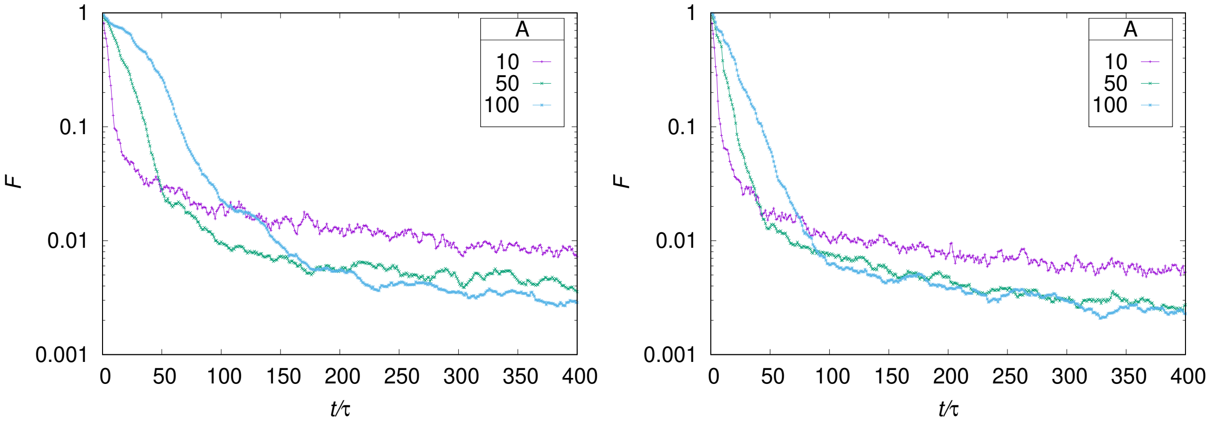

(c) $V = 1.5$ (d) $V = 5$

Figure 4.18: Evolution of fidelity, with uniform noise

In Fig. 4.18 one can observe that in the delocalised regime, the decay of $\mathscr{F}$ is exponential in t/τ with increasing rates as the width of the uniform distribution from which the kick times are drawn A reduces. This is in keeping with the notion that ballistic transport is in fact a phase coherent phenomena. However, as V increases towards V_{critical} and the break becomes more prominent, the fidelity descends sharply, before reducing indefinitely, but at a slower than exponential rate. One interesting point is that the initial rates of fidelity decay play an inconclusive role in shaping its asymptotic behaviour. Considering the case where $V = 5$, since the case with $A = 10$ sees its break from superdiffusive growth earlier than the case where $A = 100$, its early time sharp fall is mitigated, in comparison to $A = 100$ by the fact that it reaches a slow phase earlier. The slower-than-exponential decay of $\mathscr{F}$, more than one order of magnitude above its lower bound, could also possibly corroborate the evidence that this model, when the kicking is in the localised phase, is inherently robust to noise.

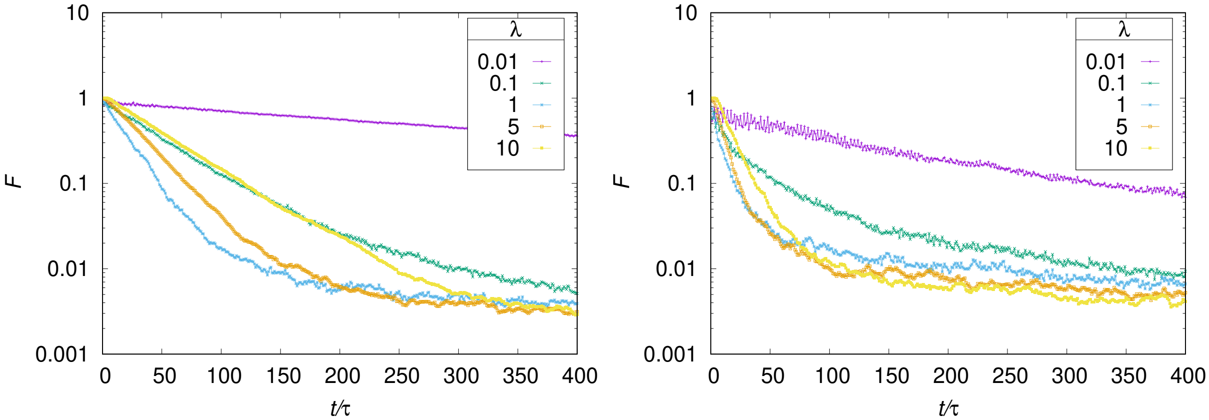

(a) $V = 0.5$ (b) $V = 0.9$

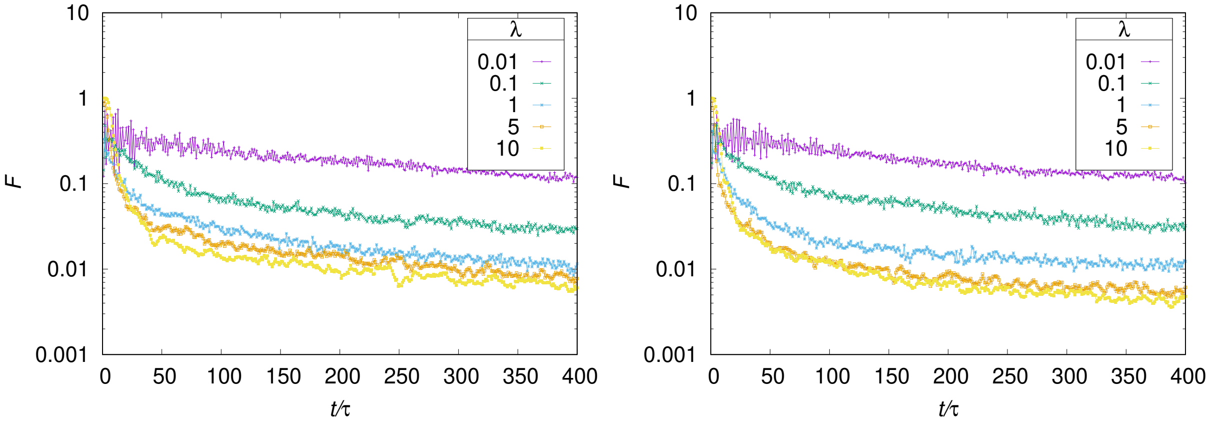

(c) $V = 1.5$ (d) $V = 5$

Figure 4.19: Evolution of fidelity, with Poisson noise

Figure 4.19 elucidates the point on the robustness to noise further. As was discussed earlier, for very small λ for the Poisson noise, the system tends to mimic the behaviour of the periodically driven system (albeit imperfectly). Deserving of particular attention is the case $\lambda = 0.01$ which shows exponential decay with a very slow rate for $V < V_{\text{critical}}$ and slower than exponential decay for $V > V_{\text{critical}}$ with increasingly severe oscillations in the transient dynamics. This reaffirms the notion that once the system has set into its mimicry of the periodic dynamics, which in the latter case is localised, the system becomes robust to decoherence, again. Some details from Fig. 4.18 are replicated as well, such as the unpredictability of asymptotic dynamics of Fidelity with knowledge of the transient behaviour in the delocalised phase. In the localised phase, however, it appears as though exponential growth is so short lived that the relative ordering of fielity is preserved through the dynamics.

4.2.4 Analysis

The analysis consists in the evaluation of $\gamma_{m=4}(t)$, defined, as in Eq. (3.13), as

$$\gamma_m(t) \equiv \frac{1}{m} \sum_{\bar{t}=-\frac{m}{2}}^{\frac{m}{2}}{}' \frac{\log\left(\sigma^2\left(t+\bar{t}\right)\right) - \log\left(\sigma^2(t)\right)}{\log\left(1+\frac{\bar{t}}{t}\right)}$$

and the fits for the (logarithms of) σ^2 vs. t/τ, so as to determine the diffusion exponents γ (i.e. γ such that $\sigma^2(t) \sim t^{\gamma}$).

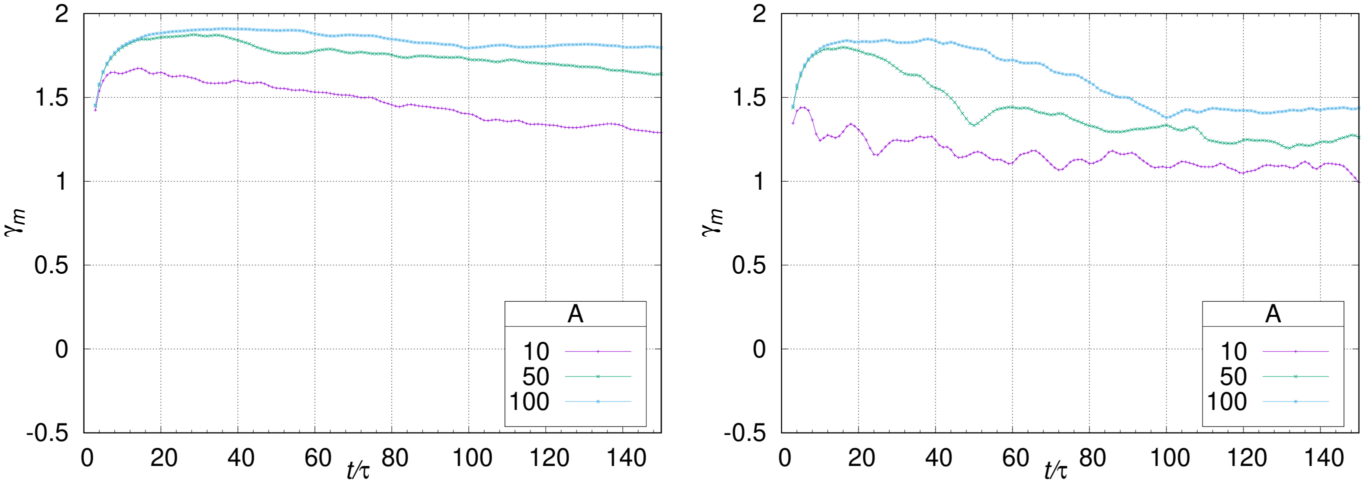

(a) $V = 0.5$

(b) $V = 0.95$

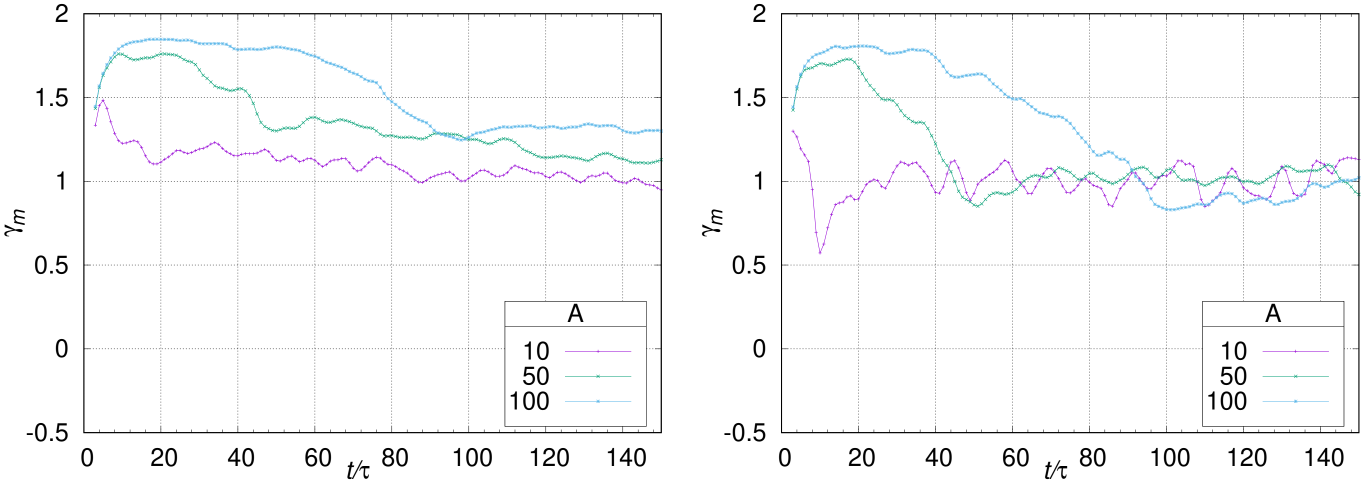

(c) $V = 1.05$

(d) $V = 1.5$

Figure 4.20: γ_4 vs. t/τ for kick times drawn from $[1, \mathrm{A}]$ at $V = 0.5, 0.95, 1.05, 1.5$

Figure 4.20 shows the emergence of a sharp break-time in the dynamics as one moves to V_{critical}. Fig. 4.20 makes clear that once V is in the localised regime, the break-time of the dynamics between superdiffusive and diffusive corresponds exactly with the value of A – the width of the uniform distribution. An even sharper agreement is seen in Fig. 4.21, the case of the 2-band model, where for $V = 1.5$, which is near the perfectly flat band $V = \frac{\pi}{2}$, and certain values of noise, the local diffusion exponent γ dips near 0 and is sometimes even negative! Again, these graphs only reinforce the open question of how flat the band must be before one starts seeing such a dip; a question which we can answer, with the data before us, as $V \in (0.5, 0.9)$, albeit without knowing which quality defines or is primarily responsible for the emergence of these dips.

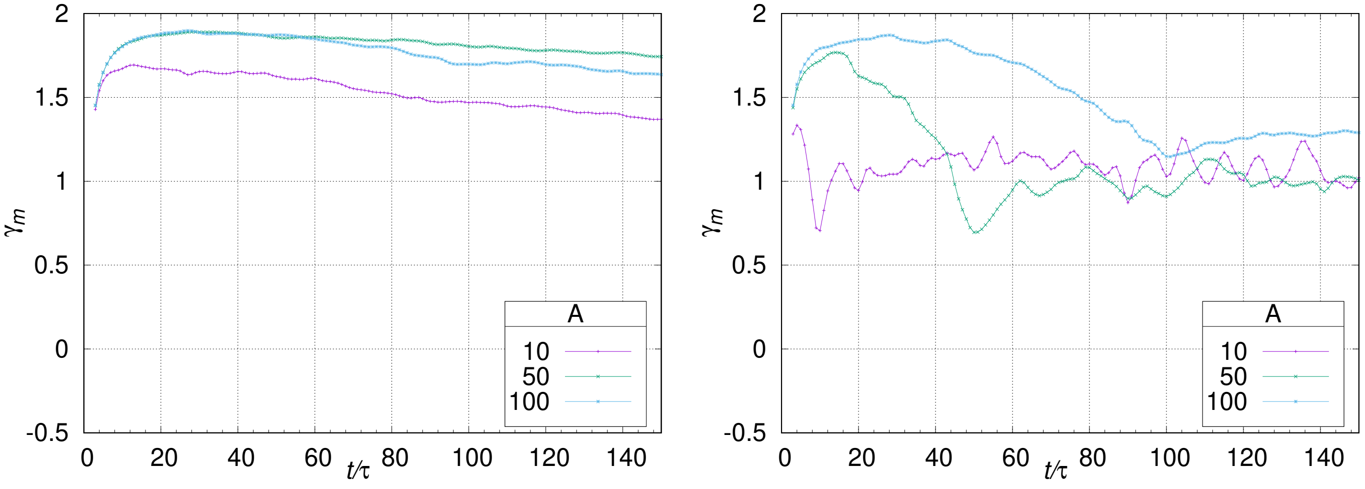

(a) $V = 0.5$ (b) $V = 0.9$

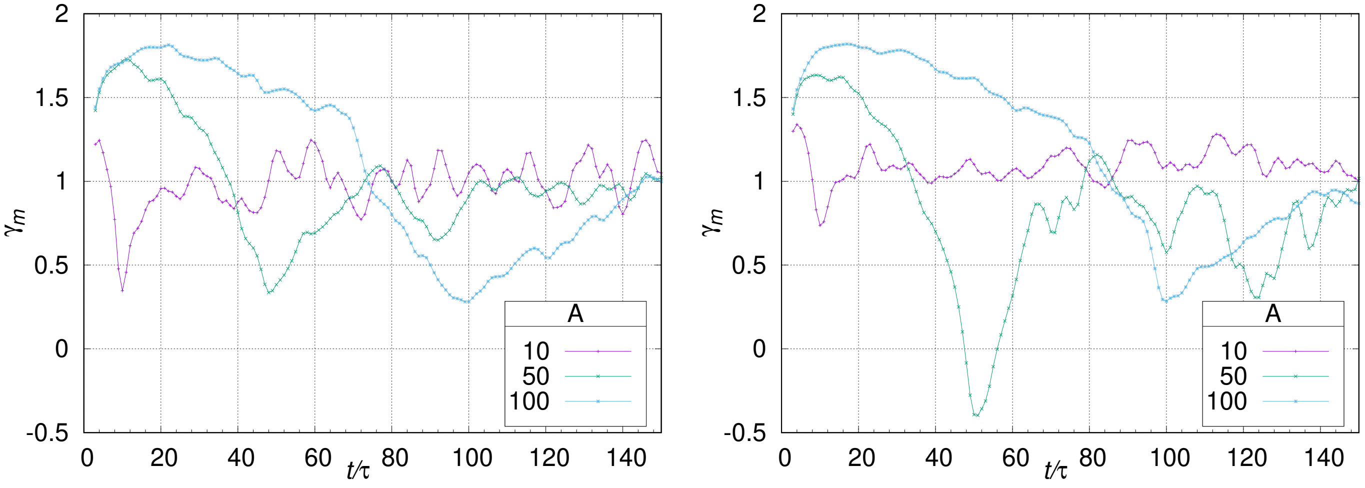

(c) $V = 1.1$ (d) $V = 1.5$

Figure 4.21: γ_4 vs. t/τ for kick times drawn from $[1, \text{A}]$ for a 2-band model

One concern with these plots is the presence of non-negligible fluctuations of γ_m as the system evolves and the impact this might have on the identification of the break-time. However, upon inspection, it should be evident that the dip surpasses all the other fluctuations in magnitude. One should be able to capture this with the calculation of a finite-difference equivalent of the second-derivative; however, the ambiguity of defining one and the difficulty with aptly averaging over a local neighbourhood of t/τ mean that it is an exercise that was considered irrelevant, for these ambiguities will likely obfuscate the possibility of there being any new information one can glean from such calculation.

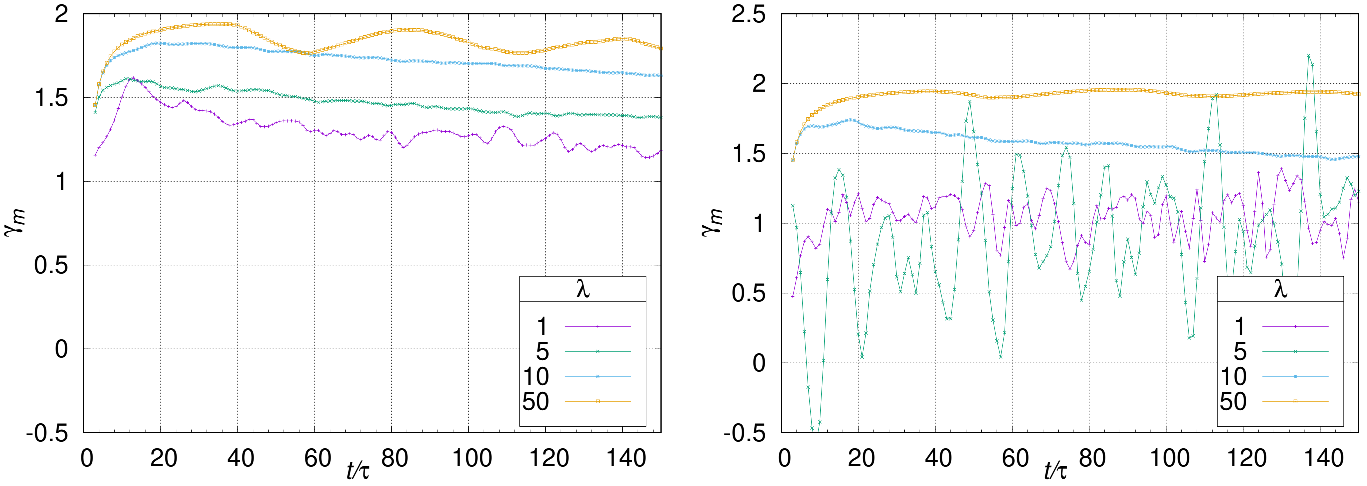

(a) $V = 0.5$, 2 band Model

(b) $V = 1.5$, 2 band Model

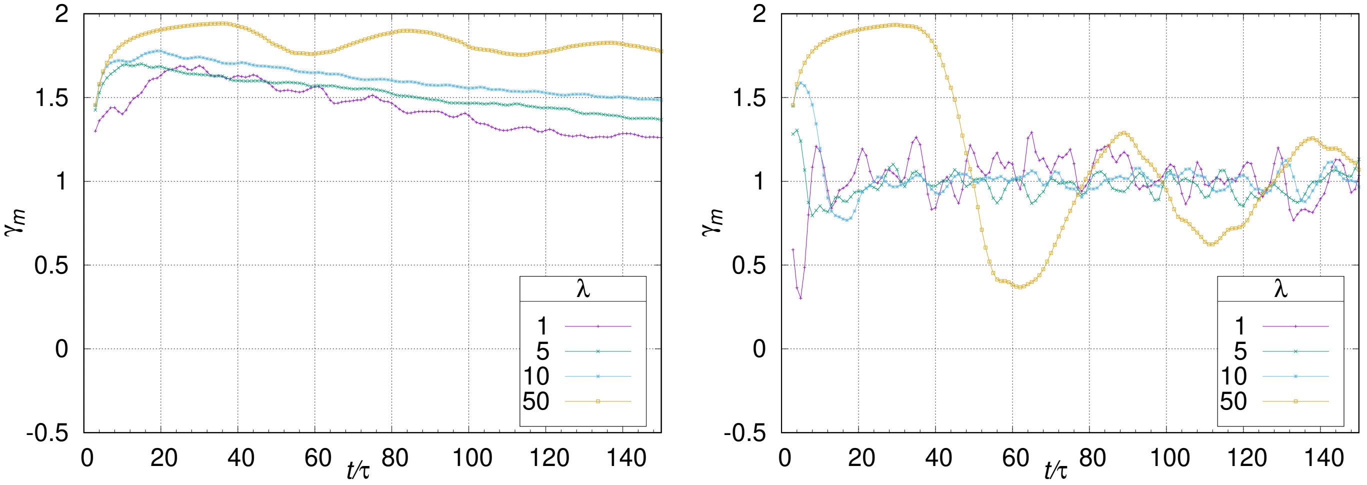

(c) $V = 0.5$, AAH Model

(d) $V = 1.5$, AAH Model

Figure 4.22: γ_4 vs. t/τ for kick times drawn from a Poisson distribution with mean λ

The same quantity is calculated for the Poisson distribution for the 2-band and the AAH model, shown in Fig. 4.22. While there is no clearly defined break-time that make itself evident from these graphs, the calculations do reveal the different qualitative regimes that occur in the dynamics of the system, depending on the mean number of timesteps between the kicks λ. For instance, in the case of the 2-band model with Poisson noise for $V = 1.5$, $\lambda = 5$ corresponds to case that oscillates before exhibiting diffusive dynamics, whereas the case with $\lambda = 1$ is diffusive from the beginning. The persistence of these regimes across potentials, related solely to the tuning of the noise, raises questions as to what the limits of applicability to tuning by noise are.

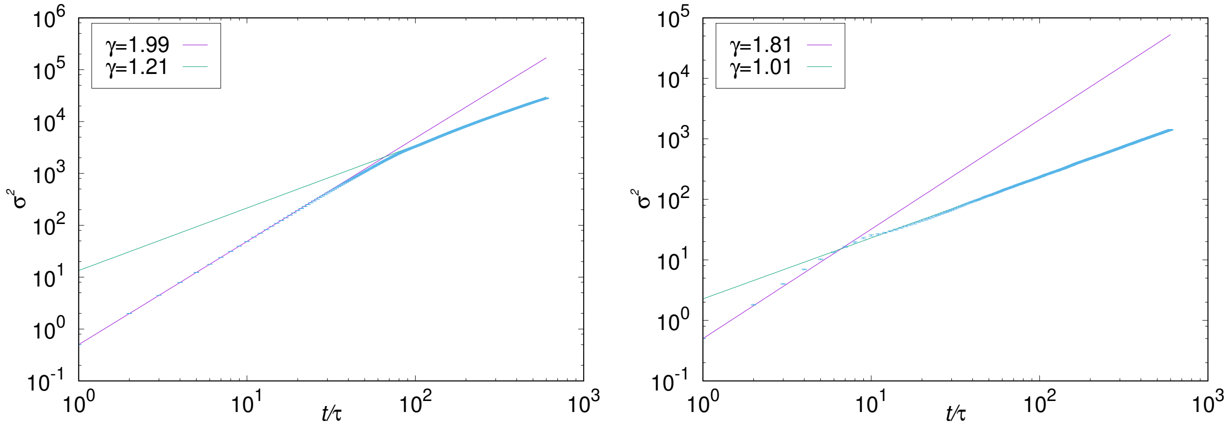

(a) $A = 100, V = 1.05$ (b) $A = 10, V = 1.5$

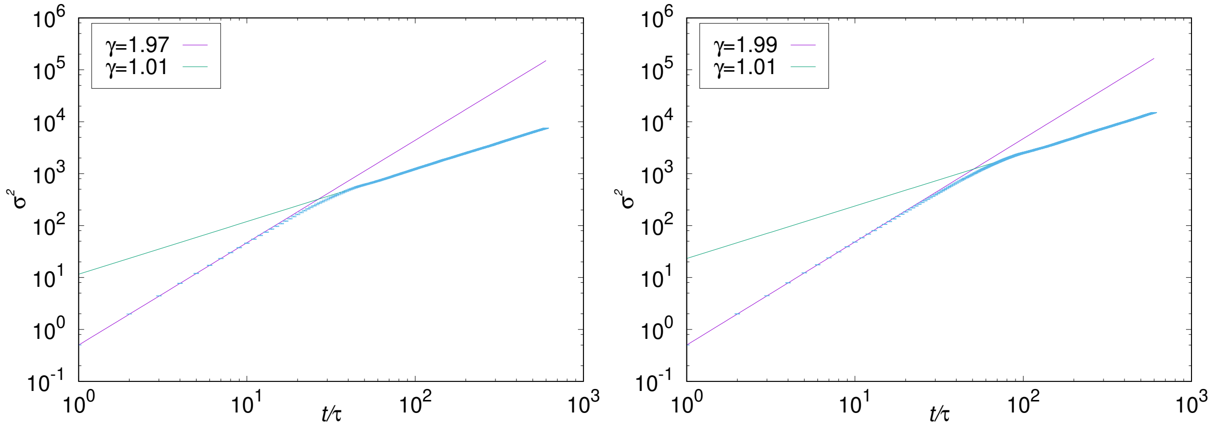

(c) $A = 50, V = 1.5$ (d) $A = 100, V = 1.5$

Figure 4.23: Fits σ^2 vs. t/τ at $A = 10, 50, 100$ for the AAH model, with uniform noise

Finally, the fits, with the best fit values of γ in the inset, are shown in Fig. 4.23. There are at least two distinct regimes in the dynamics of the system. Since in many cases the intersections of these best fit lines occur at points very close to or along the plot of σ^2, this is further evidence of the sharpness of the transition. A particularly interesting feature revealed by the fits is the presence

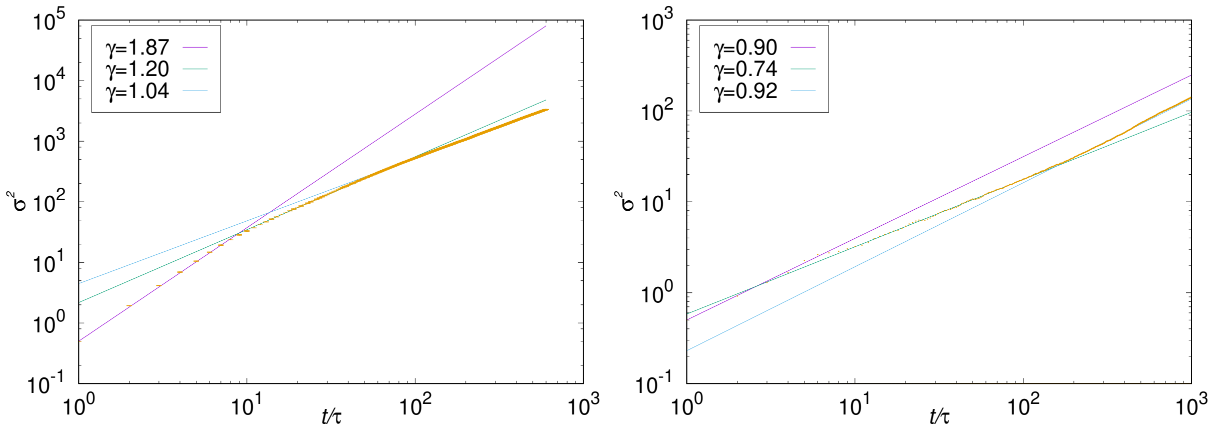

(a) $A = 10, V = 1.05$, Uniform noise

(b) $\lambda = 0.2, V = 5$, Poisson noise

Figure 4.24: Fit showing intermediate regimes for the AAH Model

of multiple regimes, as in Fig. 4.24, with the transitions between regimes still sharp.

4.2.5 Role of Noise Correlations

From the simulations, it appears as though correlations are crucial to the difference between a smooth crossover and a sharp break in the dynamics of σ^2. The correlations referred to here arise from the fact that, in general, the probabilities of there being a kick at time t and some other time $t + \Delta t$ are not going to be the same. In order to test this, the model is evolved and subject to a kick depending on the outcome of a biased coin, with various biases. The probability of there being a kick at any given instant is A.

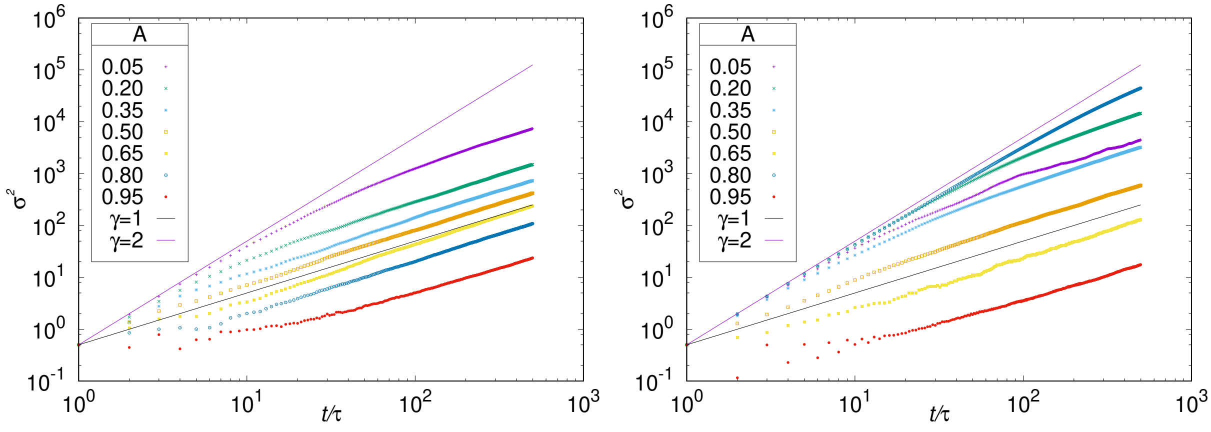

(a) AAH Model

(b) 2 band Model

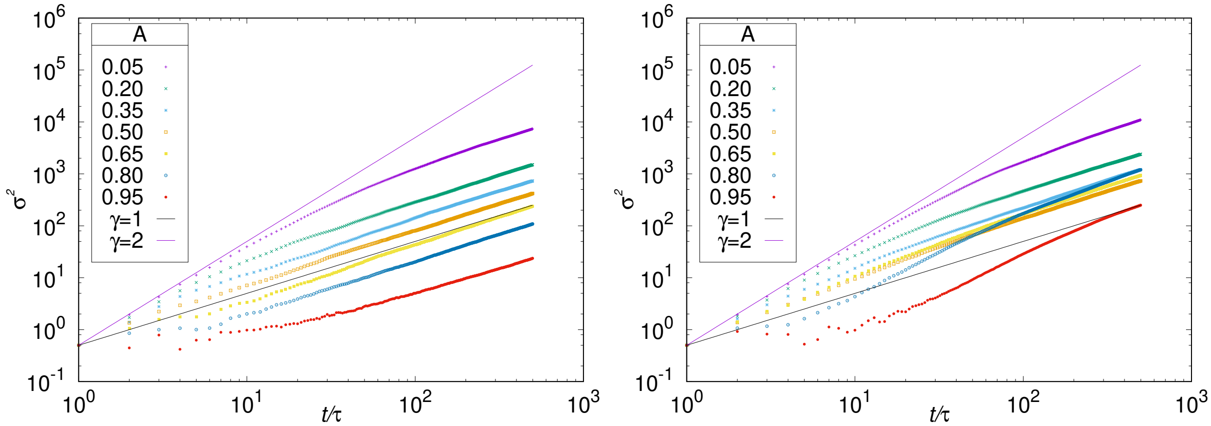

(c) 3 band model

(d) 4 band Model

Figure 4.25: σ^2 vs. t/τ at $V = 1.57$ with a coin-toss

The graphs in Fig. 4.25 show that the transition between the two dynamical regimes is smooth. This holds even when the bands are completely flat in the 2 band model.

In the 2-band case, this model has an exact solution in terms of a 4×4 "Disorder matrix". The following analysis draws on the ideas introduced in [50]. The Floquet Matrix (as given in Eq. (4.3)) is

$$F_k(\lambda) = \begin{pmatrix} \exp(\imath 2JT\cos(k))\cos(\lambda) & -\imath\sin(\lambda)\exp(\imath 2JT\cos(k)) \\ -\imath\sin(\lambda)\exp(-\imath 2JT\cos(k)) & \exp(-\imath 2JT\cos(k))\cos(\lambda) \end{pmatrix}. \tag{4.5}$$

The objective is to calculate

$$\sigma^2(N) = \overline{\langle \psi_0 | x^2(NT) | \psi_0 \rangle}; \tag{4.6}$$

$$|\psi_0\rangle \equiv \frac{1}{\sqrt{L}} \sum_k |k\rangle . \tag{4.7}$$

In the momentum representation,

$$x^2 \to \sum_{k_1,k_2} \partial_{k_1} \partial_{k_2} \delta(k_1 - k_2) \tag{4.8}$$

$$\sigma^2(N) = \sum_{\substack{\{i_n, j_n\} \\ k_1, k_2}} \langle \psi_0 | i_0 \rangle \langle j_0 | \psi_0 \rangle \overline{\left(\prod_{n=1}^{N} \langle i_{n-1} | F_{k_1}^{\dagger} | i_n \rangle \langle j_{n-1} | F_{k_1}^{T} | j_n \rangle \right)} \frac{\partial^2}{\partial k_1 \partial k_2} \delta(k_1 - k_2) \tag{4.9}$$

$$\begin{aligned} \overline{\langle i_{n-1} | F_{k_1}^{\dagger} | i_n \rangle \langle j_{n-1} | F_{k_1}^{T} | j_n \rangle} = {} & A \langle i_{n-1} | F_{k_1}^{\dagger}(\lambda) | i_n \rangle \langle j_{n-1} | F_{k_1}^{T}(\lambda) | j_n \rangle \\ & + (1 - A) \langle i_{n-1} | F_{k_1}^{\dagger}(0) | i_n \rangle \langle j_{n-1} | F_{k_1}^{T}(0) | j_n \rangle . \end{aligned} \tag{4.10}$$

One can define the following matrices

$$\begin{aligned}
D_1 &:= A\left[F_k^\dagger(\lambda)\otimes F_k^T(\lambda)\right]+(1-A)\left[F_k^\dagger(0)\otimes F_k^T(0)\right]\\
D_2 &:= A\left[F_k^\dagger(\lambda)\otimes \partial_k\left(F_k^T(\lambda)\right)\right]+(1-A)\left[F_k^\dagger(0)\otimes \partial_k(F_k^T(0))\right]\\
D_3 &:= A\left[\partial_k(F_k^\dagger(\lambda))\otimes F_k^T(\lambda)\right]+(1-A)\left[\partial_k(F_k^\dagger(0))\otimes F_k^T(0)\right]\\
D_4 &:= A\left[\partial_k(F_k^\dagger(\lambda))\otimes \partial_k(F_k^T(\lambda))\right]+(1-A)\left[\partial_k(F_k^\dagger(0))\otimes \partial_k(F_k^T(0))\right],
\end{aligned} \tag{4.11}$$

in terms of which one can express $\sigma^2(N)$ as

$$\sigma^2(N) = \\ \frac{1}{L}\sum_{\substack{i_0,j_0\\ i_N,j_N}}\sum_{n=1}^{N}\delta_{i_N,j_N}\left[D_1^{n-1}D_4D_1^{N-n}+\sum_{m=1}^{n-1}\left(D_1^{m-1}D_3D_1^{n-m-1}D_2D_1^{N-n}+D_1^{m-1}D_2D_1^{n-m-1}D_3D_1^{N-n}\right)\right]_{(i_0,j_0,i_N,j_N)}, \tag{4.12}$$

where the δ_{i_N,j_N} follows from applying $\delta(k_1-k_2)$ in the discrete limit. Certain recursion relations prove helpful in reducing the computational complexity of this evaluation to $\mathscr{O}(N)$. These are

$$A(N) = A(N-1)D_1 + D_1^{N-1}D_4; \quad A(0) := 0 \tag{4.13}$$

$$\begin{aligned}
B(N) &= B(N-1)D_1 + \widetilde{B}(N-1)D_3; \quad B(1) := 0\\
\widetilde{B}(N) &= \widetilde{B}(N-1)D_1 + D_1^{N-1}D_2; \quad \widetilde{B}(0) := 0
\end{aligned} \tag{4.14}$$

$$\begin{aligned}
C(N) &= C(N-1)D_1 + \widetilde{C}(N-1)D_2; \quad C(1) := 0\\
\widetilde{C}(N) &= \widetilde{C}(N-1)D_1 + D_1^{N-1}D_3; \quad \widetilde{C}(0) := 0
\end{aligned} \tag{4.15}$$

$$\sigma^2(N) = \frac{1}{L}\sum_{i,j}\left[A(N)+B(N)+C(N)\right]_{i,j}. \tag{4.16}$$

Note that the indices in brackets are not the true indices of the 4×4 matrix D. The recipe to switch between the two type of indices – by employing the Kronecker Product – is

$$\left[D_1^N\right]_{(i_0,j_0,i_N,j_N)} := \left[D_1^N\right]_{2(i_0-1)+j_0,2(i_N-1)+j_N}. \tag{4.17}$$

The comparison between the simulated and the calculated values of σ^2 are shown in Fig. 4.26.

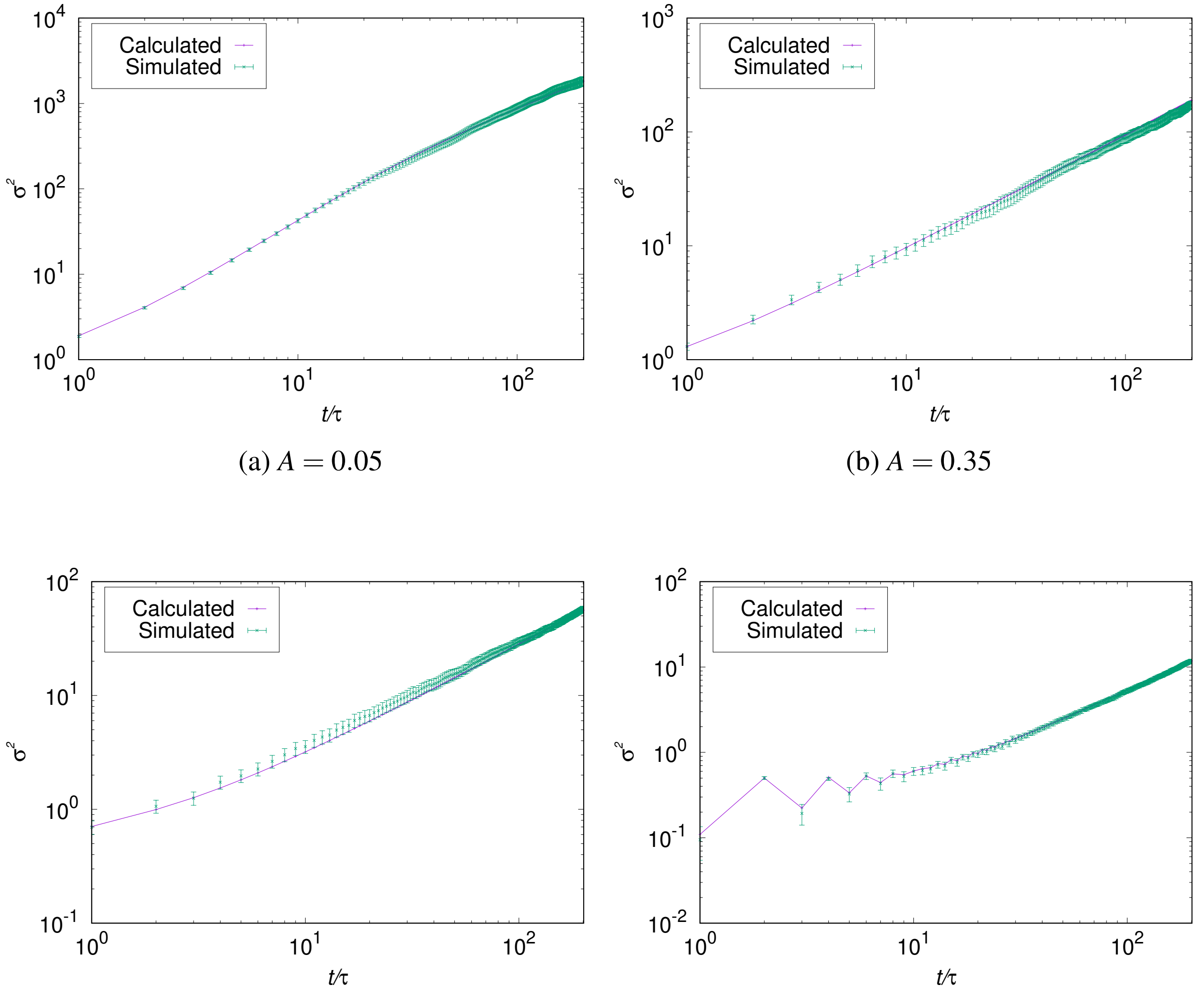

(a) $A = 0.05$

(b) $A = 0.35$

(c) $A = 0.65$

(d) $A = 0.95$

Figure 4.26: Fits of σ^2 vs. t/τ at A =0.05, 0.35, 0.65, 0.95 for the 2-band coin toss model, $V = 1.5$

The smooth nature of the crossover from the superdiffusive to the diffusive region, even at a value of V that produces sharp break-points for other correlated time of kicks seems to suggest that correlations in the noise are crucial to the sharpness in the dynamics. Indeed, there has been work on continuously, stochastically perturbed models where the correlation has played a non-trivial role in engineering such a transition [51].

Chapter 5

Take-aways and Outlook

This thesis was undertaken with the objective of unearthing the fates of localisation and transport upon introducing noise, working with a particular model – the kicked Aubry-André-Harper Model. While conventional wisdom holds that the presence of noise in a quantum system should decohere the system and lead to diffusion, the work that has been carried out in this thesis seems to suggest otherwise and appears to augment a growing body of work opposing the notion of futility of working with noisy quantum systems.

It was found that the kicked AAH Model was surprisingly robust to noise, building upon previous work that had reported similar results. Attempts to find tunable protocols that might decohere the system lead to the observation that the delivery of kicks at uniformly drawn random times leads to a sharp break in the nature of the dynamics, from superdiffusive to diffusive; the break time decided by the width of the distribution. Moving onto Poisson distributed kick times, one could see three distinct regimes of dynamics in the system. Within a given potential $V <$ or $> V_{\text{critical}}$, the regime of dynamics was decided by the properties of the noise alone, with one of the regimes identical to that of the case with uniform noise. Similar results were obtained for the normally distributed noise as well.

Interestingly, qualitatively identical results were obtained even for models possessing a discrete translation symmetry. This is interesting because the energy eigenstates for such systems are Bloch waves, which are delocalised over the extent of the system[1]. These results appear to have been brought about by a proximity to flat bands, for which it is known that there is no dynamics on the chain[2]. This also showed that flat bands could be engineered on 1-D tight-binding chain with relative ease. The parallels persist in the dynamics of the fidelity, an information theoretic measure of coherence, where systems showed, beyond an initial transient time, slower-than-exponential decay of the fidelity. Fidelity was expected to show an exponential decay generically upon the introduction of noise into the system here, but that appears not to be the case, even when no broad distributions have been set upon the system.

---

[1] Barring special cases such as flat-bands

[2] $\frac{\partial \varepsilon(k)}{\partial k} = 0 \implies v_{\text{group}} = 0$

Lastly, it was established that another crucial ingredient, in tandem with bulk localisation, was the presence of correlations in the noise in the form that times t and $t+\Delta t$ are in general not equally likely to feature kicks. This was supported by exact results for uncorrelated noise.

This litany of results with broad applicability demands, not without promise, their testing in more varied settings. The natural extensions are three fold:

Allowing Interactions

It would be interesting to observe whether such results persist in the presence of interactions. There exists a previous study [51] on noise induced subdiffusion in many-body localised systems, which reports that some results from the single-particle case do, in fact, translate. The strength of interactions, which can innately be tied to the success of a band picture in describing the system, could play a role in deciding if a break is observed. In disordered models, where many-body localisation is a possibility, it would be fitting to ask if both the sharp transitions in dynamics as well as the robustness to noise carries forth.

Correlated Kick Times

Introducing explicit correlations into the kick times provides one more parameter in manipulating the dynamics of the system. Since it is solely an external parameter, correlations often provide the best ways to engineer novel dynamics in systems with noise; a sort of order by disorder. Previous studies with correlations, both exponential [51] and broad [52], report the presence of a regime of anomalous (sub-) diffusion. In driven systems, it would be interesting to note if the sharpness persists as well.

Mobility Edges

This work has dealt exclusively with homogenous spectra, in that there are no mobility edges[3]. It has been found that periodic driving in systems with mobility edges can give rise to multifractality [53], by coupling states on either part of the spectrum. The dynamical signature of this is that as the hybridisation increases, the dynamics becomes more and more strongly subdiffusive. In the context of the present model, one might ask if it would be possible to observe a transition back to ballistic growth at late times. Moreover, localised systems often fail to ‘heat’, so interesting physics might be observed in the cases where the heating time scales are close to the time it takes to couple states across the mobility edge.

---

[3] An energy level above which all eigenstates are delocalised and below which, localised

The plenitude of directions that emerge from this work cement the fact that the nascent field of Floquet engineering via noise has much to be explored, with sufficient support from established results to serve as a point of departure. It is the hope of the author, then, that the work carried out in this thesis, hopefully aided by future analytical (even asymptotic) results, will form a foundation for further investigations in the field.

Appendix A

Code to Calculate Spread

```
#include <iostream>
#include <fstream>
#include <stdio.h>
#include <cmath>
#include <random>
#include <stdlib.h>
#include <string.h>
#include <armadillo>
#include <chrono>
#include <sys/stat.h>

using namespace std;
using namespace std::chrono;
using namespace arma;

inline bool exists_test (const std::string& name) {
struct stat buffer;
return (stat (name.c_str(), &buffer) == 0);
}

int main(int argc, char* argv[])
{
int N, R, KCK, T_tot;
```

```
double J, V_o, T;
double alph;
double A;

if(argc<=1)
{
ifstream f("pars.dat");
f>>N>>J>>V_o>>T;
f.close();
}
else
{
N=atoi(argv[1]);
J=atof(argv[2]);
V_o=atof(argv[3]);
T=atof(argv[4]);
alph1=atof(argv[5]);
KCK = atoi(argv[6]);
R = atoi(argv[7]);
T_tot=atoi(argv[8]);
}

cx_mat H(N,N,fill::zeros);
cx_vec V(N);
double rndm,s1,s2;
mat dens(N,T_tot, fill::zeros);
mat sprd(T_tot, 3, fill::zeros);
cx_vec wavefn(N);

char f_n[3][50];

sprintf(f_n[0],"expH%d.mat",N);

int i = 0; //Index
```

```
default_random_engine generator(system_clock::now().time_since_epoch().count());
//White Noise

if (exists_test(f_n[0]))
{
H.load(f_n[0]);
cout<<"Loaded\n";
}
else
{
for (; i<N-1; i++)
H(i+1,i) = H(i,i+1) = -1*J;

H(0,N-1)=H(N-1,0)=-1*J;
cout<<"Done Assigning!\n";
vec eigval;
cx_mat eigvec;

high_resolution_clock::time_point t1 = high_resolution_clock::now();
eig_sym(eigval,eigvec,H);
H=eigvec*diagmat(exp(complex<double>(0,-1)*T*eigval))*eigvec.t();

high_resolution_clock::time_point t2 = high_resolution_clock::now();

auto duration = duration_cast<seconds>( t2 - t1 ).count();
cout <<"Exponentiation "<< duration<<endl;

H.save(f_n[0]);
}

ifstream afile("A.par");
uniform_real_distribution<double> dist2(0,1);
```

```
while(afile>>f_n[2])
{
uniform_int_distribution<int> dist1(1,atoi(f_n[2])); //Replace with random number genera

rndm=dist2(generator);
for (i = 0; i<N; i++)
V(i)=exp(complex<double>(0,-1)*V_o*cos(2*datum::pi*(alph*(i+1))));

dens.fill(0.0);
sprd.fill(0.0);
for(int kck = 0; kck <KCK; kck++) //Realisations over kicks
{
wavefn.fill(0.0);
wavefn(N/2-1)=1;

int t_tot=dist1(generator), t=0;

while (t_tot<T_tot)
{
while(t<t_tot)
{
wavefn = H*wavefn;
dens.col(t)+=pow(abs(wavefn),2); //dens.col(i) represents the density at timestep -->(i+
s1=s2=0;
for(i=0; i<N;i++)
{
s1+=(i+1)*(i+1)*real(wavefn(i)*conj(wavefn(i)));
s2+=(i+1)*real(wavefn(i)*conj(wavefn(i)));
}
s1-=s2*s2;
sprd(t,0)+=s1;
sprd(t,1)+=s1*s1;
sprd(t,2)+=accu(pow(abs(wavefn),4));
t++;
}

wavefn = V%wavefn;
t_tot+=dist1(generator);
}
while(t<T_tot)
{
wavefn=H*wavefn;

dens.col(t)+=pow(abs(wavefn),2);
s1=s2=0;
for(i=0; i<N;i++)
{
s1+=(i+1)*(i+1)*real(wavefn(i)*conj(wavefn(i)));
s2+=(i+1)*real(wavefn(i)*conj(wavefn(i)));
}
s1-=s2*s2;
sprd(t,0)+=s1;
sprd(t,1)+=s1*s1;
sprd(t,2)+=accu(pow(abs(wavefn),4));

t++;
}
}

dens = dens/(KCK*R);

for(i=0;i<2;i++)
sprintf(f_n[i],"%sV%s_M%s_A%s.dat",argv[9+i],argv[3],argv[5],f_n[2]);

dens.save(f_n[0]);

sprd=sprd/KCK;
```

```
sprd.col(1)=sprd.col(1)-pow(sprd.col(0),2);
sprd.save(f_n[1],arma_ascii);

cout<<"V_o: "<<V_o<<endl;
}

return 0;

}
```

Bibliography

[1] F. L. Moore, J. C. Robinson, C. F. Bharucha, B. Sundaram, and M. G. Raizen, Phys. Rev. Lett. **75**, 4598 (1995).

[2] I. Bloch, J. Dalibard, and W. Zwerger, Rev. Mod. Phys. **80**, 885 (2008).

[3] I. Bloch, J. Dalibard, and S. Nascimbene, Nature Physics **8**, 267 (2012).

[4] A. Eckardt, Rev. Mod. Phys. **89**, 011004 (2017).

[5] L. Du, X. Zhou, and G. A. Fiete, Phys. Rev. B **95**, 035136 (2017).

[6] D. H. Dunlap and V. M. Kenkre, Phys. Rev. B **34**, 3625 (1986).

[7] P. Qin, C. Yin, and S. Chen, Phys. Rev. B **90**, 054303 (2014).

[8] C. M. Dai, W. Wang, and X. X. Yi, Phys. Rev. A **98**, 013635 (2018).

[9] W. H. Zurek, "Decoherence and the transition from quantum to classical — revisited," in *Quantum Decoherence: Poincaré Seminar 2005*, edited by B. Duplantier, J.-M. Raimond, and V. Rivasseau (Birkhäuser Basel, Basel, 2007) pp. 1–31.

[10] D. Cohen, Journal of Physics A: Mathematical and General **27**, 4805 (1994).

[11] D. Cohen, Phys. Rev. A **43**, 639 (1991).

[12] E. Ott, T. M. Antonsen, and J. D. Hanson, Phys. Rev. Lett. **53**, 2187 (1984).

[13] H. Schomerus and E. Lutz, Phys. Rev. A **77**, 062113 (2008).

[14] S. Sarkar, S. Paul, C. Vishwakarma, S. Kumar, G. Verma, M. Sainath, U. D. Rapol, and M. S. Santhanam, Phys. Rev. Lett. **118**, 174101 (2017).

[15] M. A. Nielsen and I. Chuang, "Quantum computation and quantum information," (2002).

[16] P. W. Anderson, Phys. Rev. **109**, 1492 (1958).

[17] S. Fishman, D. R. Grempel, and R. E. Prange, Phys. Rev. Lett. **49**, 509 (1982).

[18] S. Aubry and G. André, Ann. Israel Phys. Soc **3**, 18 (1980).

[19] L. Perko, *Differential equations and dynamical systems*, Vol. 7 (Springer Science & Business Media, 2013).

[20] L. Reichl, *The Transition to Chaos: Conservative Classical Systems and Quantum Manifestations* (Springer Science & Business Media, 2004).

[21] S. H. Simon, *The Oxford solid state basics* (OUP Oxford, 2013).

[22] P. Markos and C. M. Soukoulis, *Wave propagation: from electrons to photonic crystals and left-handed materials* (Princeton University Press, 2008).

[23] T. Geisel, R. Ketzmerick, and G. Petschel, Physical review letters **66**, 1651 (1991).

[24] P. G. Harper, Proceedings of the Physical Society. Section A **68**, 874 (1955).

[25] P. G. Harper, Proceedings of the Physical Society. Section A **68**, 879 (1955).

[26] D. R. Hofstadter, Phys. Rev. B **14**, 2239 (1976).

[27] B. Mandelbrot, W. Freeman, and Company, *The Fractal Geometry of Nature*, Einaudi paperbacks (Henry Holt and Company, 1983).

[28] S. Y. Jitomirskaya, Annals of Mathematics **150**, 1159 (1999).

[29] U. Kuhl and H.-J. Stöckmann, Phys. Rev. Lett. **80**, 3232 (1998).

[30] L. Ponomarenko, R. Gorbachev, G. Yu, D. Elias, R. Jalil, A. Patel, A. Mishchenko, A. Mayorov, C. Woods, J. Wallbank, *et al.*, Nature **497**, 594 (2013).

[31] B. Hunt, J. Sanchez-Yamagishi, A. Young, M. Yankowitz, B. J. LeRoy, K. Watanabe, T. Taniguchi, P. Moon, M. Koshino, P. Jarillo-Herrero, *et al.*, Science **340**, 1427 (2013).

[32] C. R. Dean, L. Wang, P. Maher, C. Forsythe, F. Ghahari, Y. Gao, J. Katoch, M. Ishigami, P. Moon, M. Koshino, *et al.*, Nature **497**, 598 (2013).

[33] Y. Lahini, R. Pugatch, F. Pozzi, M. Sorel, R. Morandotti, N. Davidson, and Y. Silberberg, Phys. Rev. Lett. **103**, 013901 (2009).

[34] R. Lima and D. Shepelyansky, Phys. Rev. Lett. **67**, 1377 (1991).

[35] R. Artuso, G. Casati, and D. Shepelyansky, Phys. Rev. Lett. **68**, 3826 (1992).

[36] R. Artuso, G. Casati, F. Borgonovi, L. Rebuzzini, and I. Guarneri, International Journal of Modern Physics B **08**, 207 (1994).

[37] T. Čadež, R. Mondaini, and P. D. Sacramento, Phys. Rev. B **96**, 144301 (2017).

[38] F. Haake and H. Haken, *Quantum signatures of chaos*, Vol. 2 (Springer, 2010).

[39] A. Gubin and L. Santos, American Journal of Physics **80**, 246 (2012).

[40] M. V. Berry and M. Tabor, Proceedings of the Royal Society of London. A. Mathematical and Physical Sciences **356**, 375 (1977).

[41] O. Bohigas, M. J. Giannoni, and C. Schmit, Phys. Rev. Lett. **52**, 1 (1984).

[42] S. N. Evangelou and J.-L. Pichard, Phys. Rev. Lett. **84**, 1643 (2000).

[43] N. Chavda, H. Deota, and V. Kota, Physics Letters A **378**, 3012 (2014).

[44] Y. Y. Atas, E. Bogomolny, O. Giraud, and G. Roux, Phys. Rev. Lett. **110**, 084101 (2013).

[45] D. Cohen, Phys. Rev. Lett. **67**, 1945 (1991).

[46] C. Sanderson and R. Curtin, Journal of Open Source Software **1**, 26 (2016).

[47] C. Sanderson and R. Curtin, in *International Congress on Mathematical Software* (Springer, 2018) pp. 422–430.

[48] Intel MKL, “Intel math kernel library,” https://software.intel.com/mkl (2018).

[49] S. H. Tekur and M. S. Santhanam, arXiv preprint arXiv:1808.08541 (2018).

[50] U. Bhattacharya, S. Maity, U. Banik, and A. Dutta, Phys. Rev. B **97**, 184308 (2018).

[51] S. Gopalakrishnan, K. R. Islam, and M. Knap, Phys. Rev. Lett. **119**, 046601 (2017).

[52] J.-P. Bouchaud and A. Georges, Physics reports **195**, 127 (1990).

[53] S. Roy, I. M. Khaymovich, A. Das, and R. Moessner, SciPost Phys. **4**, 25 (2018).